

PHOTOLUMINESCENCE SPECTROSCOPY OF CdS AND GaSe

**A THESIS SUBMITTED TO
THE GRADUATE SCHOOL OF NATURAL AND APPLIED SCIENCES
OF
THE MIDDLE EAST TECHNICAL UNIVERSITY**

BY

AYŞE SEYHAN

**IN PARTIAL FULFILLMENT OF THE REQUIREMENTS FOR THE
DEGREE
OF MASTER OF SCIENCE
IN
THE DEPARTMENT OF PHYSICS**

SEPTEMBER 2003

ABSTRACT

PHOTOLUMINESCENCE SPECTROSCOPY OF CdS AND GaSe

Seyhan, Ayşe

M. S., Department of Physics

Supervisor: Prof. Dr. Raşit Turan

September 2003, 88 pages

With the use of photoluminescence (PL) spectroscopy one can able to get a great deal of information about electronic structure and optical processes in semiconductors by the aid of optical characterization. Among various compound semiconductors, Cadmium Sulfide (CdS) and Gallium Selenide (GaSe) are interesting materials for their PL emissions. Particularly, due to its strong anisotropy, investigation of GaSe necessitates new experimental approaches to the PL technique. We have designed, fabricated and used new experimental set-up for this purpose.

In this thesis, we have investigated the PL spectra of both CdS and GaSe as a function of temperature. We observed interesting features in these samples. These features were analyzed experimentally and described by taking the band structure of the crystals into account. From the excitonic emissions, we determined the bandgap energy of both materials. We studied various peaks that appear in the PL spectra and

their origin in the material. We have found that donor acceptor transitions are effective in CdS at low temperatures. A transition giving rise to a red emission was observed and attributed to a donor level which is likely to result from an S vacancy in CdS crystal. The PL peaks with energy close to the bandgap were observed in GaSe. These peaks were attributed to the bound excitons connected either to the direct or indirect band edge of GaSe. The striking experimental finding in this work was the PL spectra of GaSe measured in different angular positions with respect to the crystal axis. We observed that PL spectra exhibit substantial differences when the angular position of the laser beam and the detector is changed. The optical anisotropy which is responsible for these differences was measured experimentally and discussed by considering the selection rules of the band states of GaSe.

Keywords: Photoluminescence, optical transitions, CdS, GaSe, optical anisotropy.

ÖZ

CdS ve GaSe’NİN FOTOLÜMİNESANS SPEKTRUMU

Seyhan, Ayşe

Yüksek Lisans, Fizik Bölümü

Tez yöneticisi: Prof. Dr. Raşit Turan

Eylül 2003, 88 sayfa

Fotoluminesans (PL) spektrumunun kullanımı ile yarıiletkenlerin elektriksel yapıları ve optiksel oluşumları hakkında büyük ölçüde bilgi edinilebilir. Kadmiyum Sulfür (CdS) ve Galyum Selen (GaSe) ilginç PL spektrumuna sahiptir. Özellikle GaSe’nin incelenmesi, sahip olduğu anisotropi nedeniyle, yeni deney düzenekler gerektirmektedir. Bu tez çalışmasında bu deney düzenekleri tasarlanmış, üretilmiş ve kullanılmıştır.

Bu tezde hem CdS hem de GaSe’nin fotoluminesans spektrumu sıcaklığa bağlı olarak incelendi. Bu maddeler hakkında ilginç sonuçlar gözlemlendi. Bu sonuçlar deneysel olarak analiz edildi ve kristallerin bant yapıları dikkate alınarak tanımlandı. Her iki kristalin enerji bandı eksitonik ışımadan faydalanılarak belirlendi. Fotoluminesans spektrumunda görülen çeşitli tepe değerleri ve muhtemel kaynakları çalışıldı. Verici - Alıcı düzey geçişlerinin düşük sıcaklıklarda CdS için etkili olduğu

bulundu. Kırmızı ışımada ortaya çıkan bir geçiş, gözlemlendi ve bu CdS kristali içindeki S boşluklarından kaynaklanan verici düzeyi olarak yorumlandı. GaSe örneğinde, enerjisi bant aralığı enerjisine yakın, fotoluminesans tepeleri gözlemlendi. Bu tepeler GaSe'nin doğrudan ya da dolaylı bant kenarlarından kaynaklı bağlı eksitonlar olarak yorumlandı. Bu çalışmadaki çarpıcı bulgu kristal eksenine göre değişik açılarda ölçülen GaSe örneğinin fotoluminesans spektrumudur. Dedektörün ve lazer ışınının açısal konumu değiştirildiği zaman fotoluminesans spektrumunda önemli değişiklikler gözlemlendi. Bu değişikliklerin nedeni olan optiksel anizotropi ölçüldü ve GaSe örneğinin bant yapısı seçme kuralları dikkate alınarak tartışıldı.

Anahtar Sözcükler: Fotoluminesans, Optiksel Geçiş, CdS, GaSe, optiksel anizotropi.

ACKNOWLEDGMENTS

I would like to express my deepest appreciation to my supervisor, Prof. Dr. Raşit Turan. Without his guidance, encouragement and support during the research, it would have been impossible for me to complete this thesis. He has always been ready to offer his help whenever needed.

I wish to thank all group members and technical staff in laboratory, especially Bülent Aslan and Uğur Serincan for being so supportive to me in difficult moments, their help in conducting experimental work and nice friendship.

I also thank Prof. Dr. Bülent Akinođlu, Assoc. Prof. Dr. Mehmet Parlak and Orhan Karabulut for providing samples.

I will always remember the supports, love, and understanding from my friends; Süreyya Yıldırım, Özlem İzci, Ayla Aldemir, Tevfik Nadi Hotamış, Evrim Uludađ, Nuray Ateş, Yasemin Sarıkaya, Nimet Uzal, Burak Uzal, İsmet Yurduşen, Sema Yurduşen, Barış Akaođlu. Thank you.

A deep sense of appreciation goes towards all of my family for providing me with the endless love and support I needed to pursue and achieve my goals in life. A very special thanks goes to İsmail Turan whose love, steadfast confidence and constant encouragement.

...TO MY FAMILY

TABLE OF CONTENTS

ABSTRACT	iii
ÖZ	v
ACKNOWLEDGMENTS	vii
TABLE OF CONTENTS	ix
LIST OF FIGURES	xi
LIST OF TABLE	xiv
CHAPTER	
1. INTRODUCTION	1
2. ELECTRONIC AND OPTICAL PROPERTIES OF SEMICONDUCTORS	6
2.1. Electronic properties of semiconductors	6
2.1.1. Band Structure.....	6
2.1.2. Holes in Semiconductors	9
2.1.3. Band Structure of Some Semiconductors	11
2.1.4. Intrinsic and Extrinsic Semiconductors	17
2.1.5. Defects	25
2.2. Optical Properties of Semiconductors	30
2.2.1. Electrons in an Electromagnetic Field	30
3. PHOTOLUMINESCENCE SPECTROSCOPY	38

3.1. Luminescence	38
3.2. Photoluminescence	39
3.3. Recombination mechanisms	41
3.3.1. Band to Band Transition	42
3.3.2. Free to Bound Transition	43
3.3.3. Donor- Acceptor Transition	44
3.3.4. Free and Bound Excitons	45
3.4. Dependence of Photoluminescence on Laser Excitation Power	47
3.5. Temperature Dependence of Photoluminescence	50
3.6. Setup of PL	53
3.7. Experimental Techniques Used in Photoluminescence Experiments.....	54
4. PHOTOLUMINESCENCE PROPERTIES OF COMPOUND SEMICONDUCTORS CdS AND GaSe	56
5. CONCLUSION	76
REFERENCES	79
APPENDIX	82

LIST OF FIGURES

FIGURES

- 2.1. Crystal structure of Si 11
- 2.2. The bandgap is 1.1 eV with the bottom of the conduction band occurring at $k=(0.852\pi/a,0,0)$ and the five other equivalent points, where a is the lattice constant (5.43 \AA)..... 12
- 2.3. The zincblende crystal structure of CdS. In the zincblende structure each(Cd,S) atom is surrounded by four (S,Cd) atoms with tetrahedral symmetry 13
- 2.4. a. Atomic confg. of GaSe. The open and the full circles represent Se atoms, Ga atoms, respectively..... 15
- 2.4. b. Perspective and top views of a unit of GaSe. 15
- 2.5. Polytype of GaSe. Crystallographic structures of the ϵ , β and γ polytypesof GaSe-like compounds. The unit cells are represented by the broken lines. They are hexagonal for the ϵ , β and rhombohedral for the γ one..... 15
- 2.6. Band structure of GaSe 17
- 2.7. A schematic of the density of states of the conduction and valence band. N_e and N_h are the electron and hole density of states. The density of electron and holes are also shown..... 18
- 2.8. As-doped Si crystal. The fifth valance electron of As is orbiting around its side.....19
- 2.9. Energy band diagram and charge concentration in n-type semiconductors.....20
- 2.10. B doped Si crystal. Substitution of Si leads to a missing electron which is indeed a hole (h^+) 20

2.11.	Energy band diagram and charge concentration in p-type semiconductor ..	21
2.12.	Energy bandgap diagram for intrinsic semiconductors with Fermi level	24
2.13.	Energy bandgap diagram for extrinsic semiconductors with Fermi level (a) for p-type, (b) for n-type.....	25
2.14.	A schematic showing some important point defect in a crystal	26
2.15.	Shottky and Frenkel defects.....	27
2.16.	Schematic presentation of a dislocation; the last row of atoms (dark) in the inserted fractional plane	28
3.1.	Most common radiative transition observable with photoluminescence and non-radiative transitions.....	40
3.2.	Most common radiative transition observable with photoluminescence and non-radiative transitions.....	42
3.3.	The schematic representation of Photoluminescence set-up	52
3.4.	Holders.....	54
4.1.	Photoluminescence spectrum of CdS at $T \sim 20$ K.....	57
4.2.	PL spectra of green band of CdS as a function of temperature	58
4.3.	PL spectra of the near band edge transitions of CdS as a function of temperature	59
4.4.	PL spectra of red band for CdS as a function of temperature.....	59
4.5.	Optical transition in CdS crystal.....	60
4.6.	Temperature dependences of red band CdS PL intensity at the emission band maxima.....	62
4.7.	Deconvolution of the photoluminescence spectra into Gaussian lineshapes at ~ 20 K. (k//c).....	64
4.8.	Variation of GaSe PL intensity with reciprocal temperature, at 20 and 300 K.....	65
4.9.	Temperature dependence of the peak energy position of the A band	66
4.10.	Photoluminescence spectra of undoped p-type GaSe as a function of temperature. k//c.	67

4.11.	Experimental conditions for the measurement of anisotropic PL emission. a) Laser beam is directed to the sample surface with an angle of 45° with respect to c-axis. The detector is positioned along the c-axis ($k//c$). b) Laser beam is directed on the side of the sample. The detector's position is along the direction perpendicular to the c-axis ($c \perp k$). c) The detector is in the same position as b), but the laser beam falls on the sample with an angle	69
4.12.	Photoluminescence spectrum of GaSe with respect to $k//c$ and $k \perp c$ axis	70
4.13.	Photoluminescence spectra of GaSe as a function of temperature. $k \perp c$.	71
4.14.	Photoluminescence spectra of GaSe as a function of temperature. $k \perp c$.	71
4.15.	Deconvolution of the photoluminescence spectra into Gaussian lineshapes at ~ 20 K. $k \perp c$	73
4.16.	Variation of GaSe PL intensity with reciprocal temperature, $k \perp c$	74
4.17.	Temperature dependence of the peak energy position, $k \perp c$	75

LIST OF TABLES

TABLES

2.1	Effective mass of carriers in germanium, silicon Crystal structure of Si ..	8
2.2.	Fitting parameters for Germanium and Silicon	9
2.3.	Some properties of Si. All temperature dependent parameters are at T=300K [11].	13
2.4.	Some propetties of CdS [11]......	14

CHAPTER 1

INTRODUCTION

During the seventies and eighties, we have witnessed remarkable advances in our understanding of semiconductor properties and rapidly expanding uses of semiconductor devices in industrial and consumer products. The phenomenal growth of the semiconductor industry has resulted in a gradual increase in material research for better, higher performance, and more reliable semiconductors. The questions regarding degradation of semiconductor device performance rely on heavily on our basic knowledge of semiconductor materials such as that which relates to carrier transport, defect mechanism and impurities. For different semiconductor devices, one needs materials with different parameters, like energy gap. Physical properties are very different among different semiconductors due to distinct characteristics of energy gaps and impurities. These impurities play a major role in determining the electrical and optical properties of semiconductors. One of the most commonly used techniques to investigate properties in semiconductors is Photoluminescence.

Photoluminescence (PL) has become a standard method for the characterization of semiconductors properties. It combines the advantages of an optical method, namely being non-destructive and not requiring electrical contacts, with very high sensitivity. PL can be used to determine energy levels, concentration

of impurities, defects and fundamental properties of semiconductors [1, 2]. PL, more generally all kind of luminescences, is a result of energy transition of electrons. Photoluminescent materials are characterized primarily on the basis of the mechanism(s) involved in (1) interband transitions, (2) transition including impurities or defects and (3) hot carrier intraband transitions. The first category is further broken down into near band edge band-to-band transition, and hot carrier band-to-band transition. Second category consists of conduction band to acceptor level, donor level to valance band, donor to acceptor level transition, free and bound exciton transition, and deep level transition. All these transitions could result in the emission of photon; whether this is likely or not depends on both the transition mechanism and the material. Many other considerations serve to further complicate this already complex topic. An electron and a hole orbit each other about their common center of mass; this hydrogen-atom-like system is called an exciton. Exciton can only exist for a meaningful length of time at very low temperatures. Since the electron and the hole attract each other, an exciton has less potential energy than a free pair of charge carriers. Thus when an exciton recombines, any photon which is emitted has slightly less energy than the bandgap. Since this photon doesn't have quite enough energy to re-excite an electron from the valance band into conduction band, it has a much better chance to escape from the crystal than photons created by transition at or above the bandgap.

The basic difference between direct gap and indirect gap transitions is that, unlike for indirect gap case, the maximum of valance band and minimum of the conduction band occur for the same value of the wave number k for direct gap transitions. Because the electron will tend to equilibrate to the lowest energy state

available, the top of the valance band will collect holes, as electrons move down into available lower energy states. For the same reason, the bottom of the conduction band will collect electrons. Thus in a material with a direct gap the k values of these distributions overlap and photons can be emitted as carriers recombine directly. On the other hand, in a material with an indirect gap the story is not that much simple, since a transition from conduction band to the valance band involving only the emission of a photon will not conserve the crystal momentum. In order for an electron to make a transition from to conduction to the valance band, both a photon and a phonon may be emitted thus allowing both momentum and energy to be conserved. In this thesis we studied PL technique by conducting on compound semiconductors Cadmium Sulfide (CdS) and Gallium Selenide (GaSe) as a function of temperature.

Bulk cadmium sulfide has both wurtzite crystal structure, especially when grown at high temperature and zinblende crystal structure when precipitated from solution [3]. The Cd-S bonds in the crystal have both ionic and covalent character. Bulk CdS is nearly always n-type semiconductors, having in their natural state a preponderance of electron donor states near the conduction band edge [4]. The band gap energy of CdS is given in [5] at $T=300$ K and $T=0$ K the bandgap energies are 2.53eV (491nm), and 2.58eV (481nm), respectively.

The experimental investigation of the electrical and optical properties of GaSe has received much attention due to its possible application in photoelectronic devices in the visible range [6]. Being a member of the group III-VI, GaSe is a layer semiconductor whose crystal c -axis is perpendicular to the layer planes. The sandwich layer consists of four covalently bound sheets of hexagonal close-packed

atoms, arranged in the sequence Se-Ga-Ga-Se [7]. Three different periodic stacking sequence of the layers have so far been observed and have been described in the literature as ϵ , γ , and β - GaSe. The ϵ and β - phases are 2H Hexagonal polytypes, and the modification γ has a 3R trigonal structure [8]. The layers are bound by weak van der Waals forces while intralayer –bonding forces are primarily ionic-covalent in nature. The electronic band structure of GaSe shows indirect minimum of the conduction band (CB) at the M point of the Brillouin zone which is lower (only 25meV) than the direct gap at the Γ point and they are located the top of the valance band (VB) at the center of the Brillouin zone [9]. PL of GaSe is highly complex at low temperature; it involves either intrinsic sharp lines because of the excitonic recombination or extrinsic bands at lower energy related to the lattice defects or impurities.

Organization of this thesis is as follows. In chapter 2, as a theoretical background material to our experimental investigation, electronic and optical properties of semiconductors are comprehensively reviewed. We particularly deal with the basics of electrons and holes in semiconductors, band structure of semiconductors and present further band structure for some specific semiconductors. The properties of conduction and valance bandedge states, intrinsic and extrinsic semiconductors and defects in semiconductors are also briefly discussed. In the last part of this chapter we concentrate on the motion of an electron in an electromagnetic field by focusing on its optical parameters.

In the next chapter after brief discussion of luminescence and photoluminescence concepts, we present the recombination mechanisms such as band to band transition, free to bound transition, donor-acceptor transition, and free

and bound excitons. Next the dependencies of the photoluminescence spectrum on the parameters such as the laser excitation power and temperature are discussed separately in a general sense. Chapter 3 is finalized by depicting a schematic representation of a PL setup that we have used in our experimental survey.

In the subsequent chapter, chapter 4, photoluminescence properties of our sample crystals CdS and GaSe are investigated separately. Firstly, we have carried out PL spectroscopy of CdS in the temperature range of 0 -300 K. Set-up used in this investigation is shown in Fig. (3.3). A series of PL peaks were observed with the peak values located at approximately 490 nm, 696 nm, and 449nm. The bandgap of CdS is divided into four fundamental bands which are labeled as Green, Yellow, Red and Raman. We observed five of all peaks in the Green band. The observed peak values are almost in agreement with those already exist in literature. There is only one peak in red band, we interpret the peak as the one originated from deep level created by S vacancies. The peak energy appears at 696 nm. The last peak known as Raman, located at 449 nm in the temperature range from 130-20 K.

Secondly, PL spectrum of GaSe was studied. Having electrical and optical anisotropy, GaSe has quite complex band structure like CdS. PL spectrum of GaSe shows a large number of sharp lines near the band edge and wider bands away from the band edge. This is the case since both direct and indirect transitions are likely to occur. Free and bound exciton transitions were observed in each of direct and indirect bandgap at 606 and 627 nm, respectively. There exists one more peak in the temperature region 70-20 K at 647 nm. Final chapter of the thesis is devoted to our conclusions.

CHAPTER 2

THEORETICAL APPROACH:

ELECTRONIC AND OPTICAL PROPERTIES OF SEMICONDUCTORS

2.1 ELECTRONIC PROPERTIES OF SEMICONDUCTORS

Semiconductor is a material whose electrical conductivity is midway between that of a good conductor and a good insulator; a type of material having a lower energy valence band that is nearly completely filled with electrons and a higher energy conduction band that is nearly completely empty of electrons, with a modest energy gap between the two bands; pure materials usually exhibit electrical conductivity that increases with temperature because of an increase in the number of charge carriers being promoted to the conduction band.

2.1.1 Band Structure

Energy bands consisting of a large number of closely spaced energy levels exist in crystalline materials. The bands can be thought of as the collection of the individual energy levels of electrons surrounding each atom. The wavefunctions of the individual electrons, however, overlap with those of electrons which is confined to neighboring atoms. The Pauli exclusion principle does not allow the electron energy levels to be the same so that one obtains a set of closely spaced energy levels, forming an energy band. The energy band model is crucial to any detailed treatment

of semiconductor devices. It provides the framework needed to understand the concept of an energy bandgap and that of conduction in an almost filled band as described by the empty states.

The analysis of periodic potentials is required to find the energy levels in a semiconductor. This requires the use of periodic wave functions, called Bloch functions. The description of the electron in a semiconductor has to be done via the Schrodinger equation

$$\left(-\frac{\hbar^2}{2m_0} \nabla^2 + U(r) \right) \psi(r) = E \psi(r), \quad (2.1)$$

where $U(r)$ is the background potential seen by the electrons. The Bloch theorem gives us the form of electron wavefunction in a periodic structure and it states that the eigenfunction is the product of a plane wave $e^{ik \cdot \vec{r}}$ times a function $u_k(r)$ which has the same periodicity as the periodic potential. Thus,

$$\psi_k(r) = e^{ik \cdot \vec{r}} u_k(r), \quad (2.2)$$

is the form of the electronic function. With this way, the energy levels are grouped in bands which are separated by energy band gaps. The behavior of electrons at the top and bottom of such a band is almost same as that of a free electron. However, the electrons are affected by the presence of the periodic potential. This effect can be involved into the theory by redefining the mass of the electron to a different value. This mass will be referred to as the effective mass.

It is reasonable that electrons with an energy close to a band minimum can be considered as free electrons and they accelerate in an applied electric field just like a free electron in vacuum. Their wavefunctions are periodic and extend over the size of the material. The potential is periodic due to the atoms in the crystal without the

valence electrons and, as noted before, it has effects on the properties of the electrons. Therefore, the mass of the electron differs from the free electron mass, m_0 . Because of the anisotropy of the effective mass and the presence of multiple equivalent band minima, it is needed to define two types of effective mass which are the effective mass for density of states calculations and the effective mass for conductivity calculations, respectively. In Table 2.1, we give the effective mass values for electrons and holes for two semiconductors.

Table 2.1 Effective mass of carriers in germanium, silicon.

		Si	Ge
Electron effective mass for conductivity calculations	$\frac{m_{e,con}^*}{m_0}$	0.12	0.26
Electron effective mass for density of states calculations	$\frac{m_{e,dos}^*}{m_0}$	0.55	1.08
Hole effective mass for conductivity calculations	$\frac{m_{h,con}^*}{m_0}$	0.21	0.386
Hole effective mass for density of states calculations	$\frac{m_{h,dos}^*}{m_0}$	0.37	0.811

The energy bandgap of semiconductors tends to decrease as the temperature is increased. This behavior can be better understood if one considers that the interatomic spacing increases when the amplitude of the atomic vibrations increases due to the increased thermal energy. This effect is quantified by the linear expansion

coefficient of a material. An increase in interatomic spacing decreases the average potential seen by the electrons in the material, which consequently reduces the size of the energy bandgap. A direct modulation of the interatomic distance - such as by applying compressive stress - also causes an increase (decrease) of the bandgap.

The temperature dependence of the energy bandgap, E_g has been experimentally determined and its dependency can be expressed as of the form:

$$E_g(T) = E_g(0) - \frac{\alpha T^2}{T + \beta}, \quad (2.3)$$

where $E_g(0)$, α and β are the fitting parameters. These fitting parameters are listed for germanium and silicon in Table 2.2.

Table 2.2 Fitting parameters for Germanium and Silicon

	Germanium	Silicon
$E_g(0)(eV)$	0.7437	1.166
α (meV/K)	0.477	0.473
β (K)	235	636

2.1.3 Holes in semiconductors

Semiconductors differ from metals and insulators by the fact that they contain an empty conduction band and a full valence band at 0 K. At finite temperature some of electrons leave the valence band and occupy the conduction band. The valence band is then left with some unoccupied states [10].

If all the valence band states are occupied, the sum over all wavevector states is zero,

$$\sum k_i = 0 = \sum_{k_i \neq k_e} k_i + k_e . \quad (2.4)$$

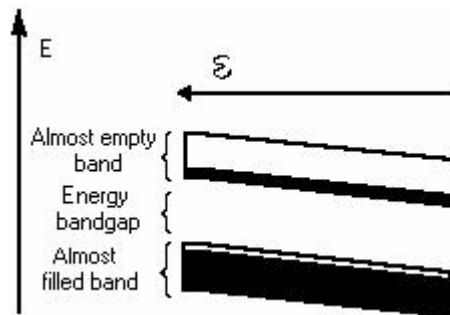
This result shows us that there are as many positive k states occupied as negative. Therefore if we have a situation where the electron at wavevector k_e is missing, the total wavevector is not equal to zero but it yields

$$\sum_{k_i \neq k_e} k_i = -k_e . \quad (2.5)$$

The missing state is called a hole and the wavevector of the system $-k_e$ is assigned to it. It is note that the electron is missing from the state $-k_e$ and the momentum associated with the hole is at $-k_e$. The position of the hole is depicted as that of the missing electron. But reality the hole wavevector k_h is equal to $-k_e$,

$$k_i = -k_e . \quad (2.6)$$

If the electron is not missing the valance band electrons cannot carry any current. However, there will be a current flow, if an electron is missing. When an electric field is applied, all the electrons move in the direction opposite to the electric field



and this results in the unoccupied state moving in the field direction. This means that the hole thus behaves as if it has a positive charge. The dynamics of a hole state under an external electromagnetic field can be governed by the following equation of motion

$$\hbar \frac{d\vec{k}_h}{dt} = e(\vec{E} + \vec{v}_h \times \vec{B}), \quad (2.7)$$

where E and B refer to electric and magnetic fields, and $\hbar\vec{k}_h$ and \vec{v}_h are the momentum and velocity of the holes, respectively. Thus, the equation of motion of holes is nothing but that of a particle with a positive charge e. The mass of holes has a positive value, although the electron mass in its valance band is negative.

2.1.4 Band Structure of Some Semiconductors

2.1.4.1 Silicon:

Nowadays, silicon is one of the most widely used semiconductors. In addition to processing higher band gap energy, the natural oxide of silicon also makes the manufacture of semiconductor device comparatively easy. One of the main reasons for the popularity of silicon is that it is stable and can be heated to a rather high degree by keeping its material characteristics. If we consider the lattice structure of Si, it has a diamond shape and each atom in the diamond lattice has a covalent bond with four adjacent atoms, which together form a tetrahedron. This structure is shown in Fig.2.1.

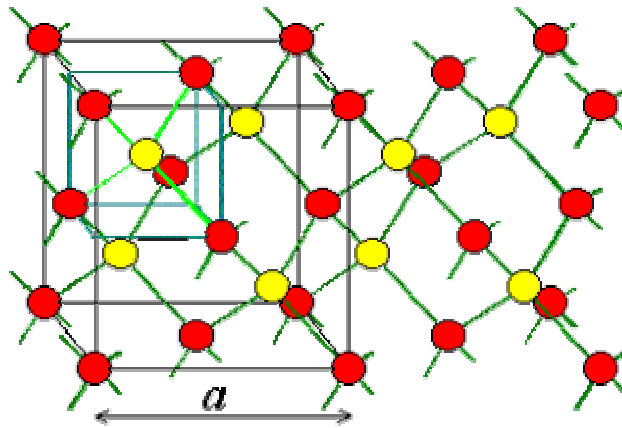


Fig.2.1 Crystal structure of Si.

The band structure of Si is shown in the Fig.2.2:

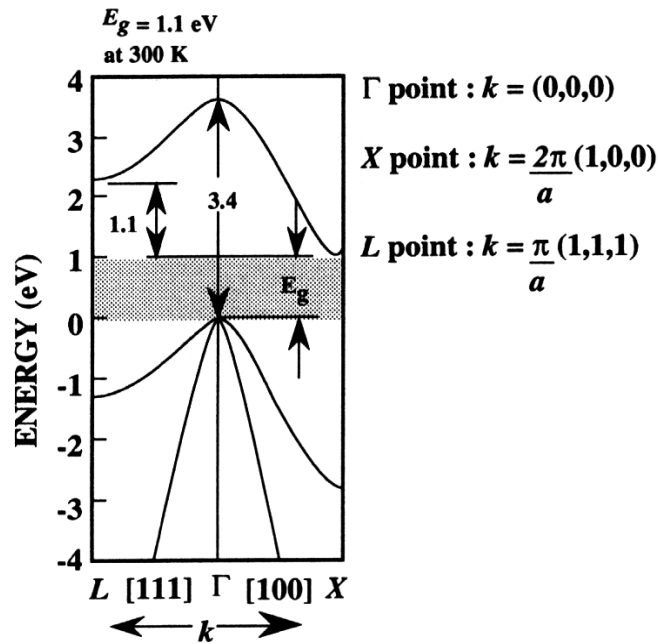


Fig.2.2 The bandgap is 1.1 eV with the bottom of the conduction band occurring at $k = (0.852\pi/a, 0, 0)$ and the five other equivalent points, where a is the lattice constant (5.43 \AA) [10].

The band structure near the conduction minima is

$$E(k) = \frac{\hbar^2 k_l^2}{2 m_l^*} + \frac{\hbar^2 k_t^2}{2 m_t^*}, \quad (2.8)$$

where $m_l^* = 0.98m_0$ and $m_t^* = 0.19m_0$, and gives ellipsoid constant energy surfaces.

Note that in Eq. (2.8) k is measured from the band edge value. Some properties of Si are given in Table (2.3).

Table.2.3 Some properties of Si. All temperature dependent parameters are at $T=300K$ [11].

Atomic Weight	28.09
Breakdown field (V/cm)	$\sim 3E5$
Crystal structure	Diamond
Density (g/cm ³)	2.328
Dielectric Constant	11.9
N_c (cm ⁻³)	$2.8E19$
N_v (cm ⁻³)	$1.04E19$
Effective Mass, m^*/m_0 Electrons m_l^*, m_t^* Holes m_{ch}^*, m_{hh}^*	0.98, 0.19 0.16, 0.49
Electron affinity, χ (V)	4.05
Energy gap (eV) at 300K	1.12
Intrinsic carrier conc. (cm ⁻³)	$1.45E10$
Intrinsic Debye Length (μm)	24
Intrinsic resistivity ($\Omega\text{-cm}$)	$2.3E5$
Lattice constant (Å)	5.43095
Linear coefficient of thermal expansion, $L/LT(C^{-1})$	$2.6E-6$
Melting point (C)	1415
Minority carrier lifetime (s)	$2.5E-3$
Mobility (drift) (cm ² /V-s)	1500 450
Optical-phonon energy (eV)	0.063
Phonon mean free path (Å)	76(electron) 55(hole)
Specific heat (J/g C)	0.7
Thermal conductivity (W/cmC)	1.5
Thermal diffusivity (cm ² /s)	0.9
Vapor pressure (Pa)	1 at 1650C $1E-6$ at 900 C

2.1.4.2 CdS

The II-VI compounds of CdS have direct band gaps. CdS has commonly zincblende crystal structure. This is especially the case when it is grown at high temperature but it is possible to grow wurtzite crystal as well. The Cd-S bonds in such crystal show both ionic and covalent character. Bulk CdS is nearly always n-type semiconductors.

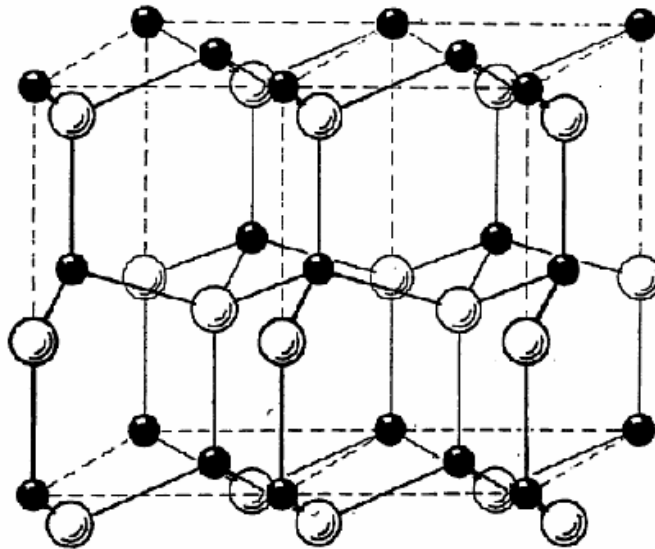


Fig.2.3 The zincblende crystal structure of CdS. In the zincblende structure each (Cd, S) atom is surrounded by four (S, Cd) atoms with tetrahedral symmetry.

Table.2.4 Some propetties of CdS [11].

Atoms/cm ³	4.0237E22
Atomic Weight	144.46
Crystal structure	Zincblende
Density (g/cm ³)	4.826
Dielectric Constant, static	5.4
Effective Mass, m [*] /m ₀	
Electrons	0.165
Holes m [*] _{lh} , m [*] _{hh}	
Energy gap (eV) at 300K	2.42
Lattice constant (Å)	5.832
Melting point (C)	1477
Mobility (drift) (cm ² /V-s)	
electron	340
hole	50

2.1.4.3 Crystal and Band Structure of GaSe

The covalently bounded layers of the III-VI compound GaSe contain four monatomic sheets in the order Se-Ga-Ga-Se. Each single layer is hexagonal and the c-axis is perpendicular to the layer plane. Atomic configuration of a GaSe layered semiconductor as follows:

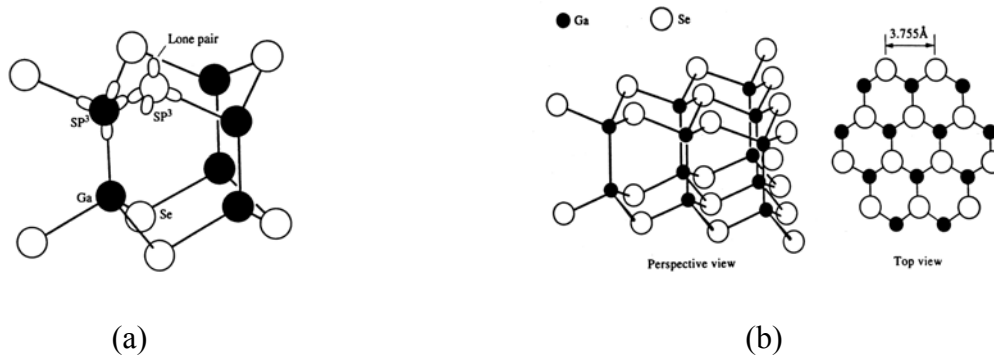


Fig.2.4 (a) Atomic config. of GaSe. The open and the full circles represent Se atoms, Ga atoms, respectively [12]. (b) Perspective and top views of a unit of GaSe [13].

Depending on the period of stacking sequences there are four modifications: ϵ , β , γ and δ . [14]. The ϵ and β modifications are 2H hexagonal type and γ and δ are 3R trigonal type [15].

The layer compounds consist of sheets which stick to each other to form a three dimensional crystal. The thickness of sheets is about a few atoms. The bonding between the atoms of a single layer is covalent and each layer forms a self contained crystalline unit. Bondings among different layers are formed by weaker forces such as Van der Waals with some ionic or coulomb contributions. Since there exists highly asymmetric charge distribution surrounding the atoms, the combination of strong and weak bands in the structure of the layer compounds result in anisotropic [15, 17, 18].

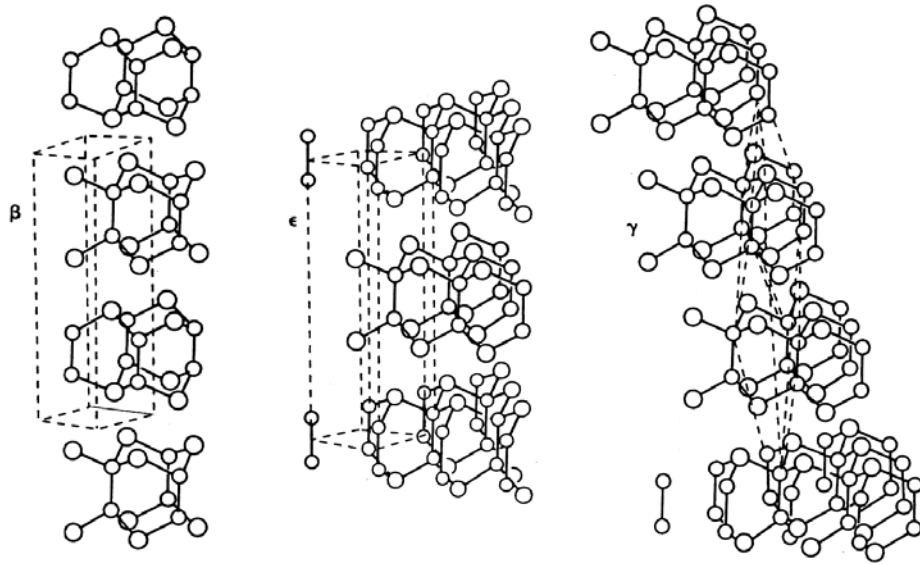


Fig.2.5 Polytype of GaSe. Crystallographic structures of the ϵ , β and γ polytypes of GaSe-like compounds. The unit cells are represented by the broken lines. They are hexagonal for the ϵ , β and rhombohedral for the γ one [16].

The electronic band structure of GaSe, calculated by the empirical pseudopotential method [14, 19, 20] shows the existence of a low-lying indirect minimum of conduction band (CB) at the M point of Brillouin zone which is lower than the direct one at the Γ point and they located the top of the valance band (VB) at the center of the Brillouin zone. Optical transition between the VB and the direct and the indirect minima in the CB are allowed with various strengths depending on the polarization of the light. While the indirect gap energy in GaSe is 2.102 eV at 4.2 K [17], the direct gap energy becomes 2.128 eV at 4.2 K and 2.021eV at 300K.

GaSe is highly transparent in the infrared region between the wavelengths 0.65 – 18 μm . At room temperature its resistivity is 100 ohm-cm, hall coefficient of about $3000\text{cm}^3/\text{coloumb}$, and mobility $30\text{ cm}^2/\text{V}$ [21].

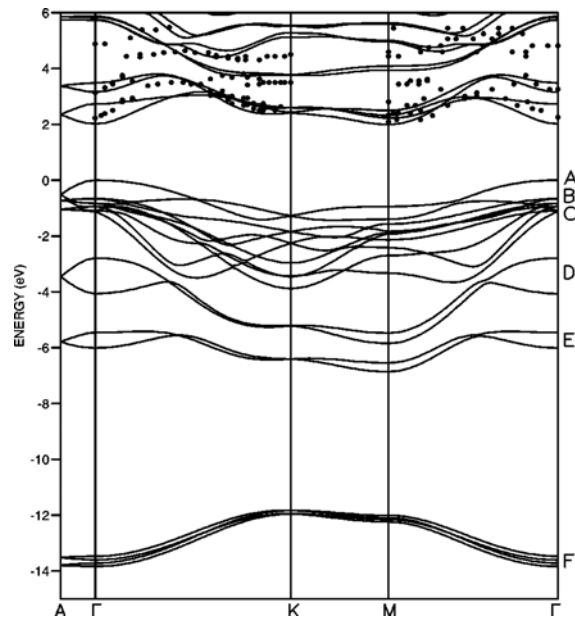


Fig.2.6 Band structure of GaSe.

2.1.5 Intrinsic and Extrinsic Semiconductors

Intrinsic semiconductors:

The aim in semiconductors technology is to first purify the material as much as possible and then introduce impurities in a controlled way. We call the pure semiconductors “*intrinsic*”, and we call the semiconductor “*extrinsic*” after external interference has changed its inherent properties. In devices extrinsic semiconductors are mostly used, but it is better to start dealing with the intrinsic semiconductors first.

The intrinsic carrier concentration depends on the parameters of semiconductors such as the bandgap, temperature and the detail of the band edge masses. The conduction and valence band density of states are shown in Fig. (2.6).

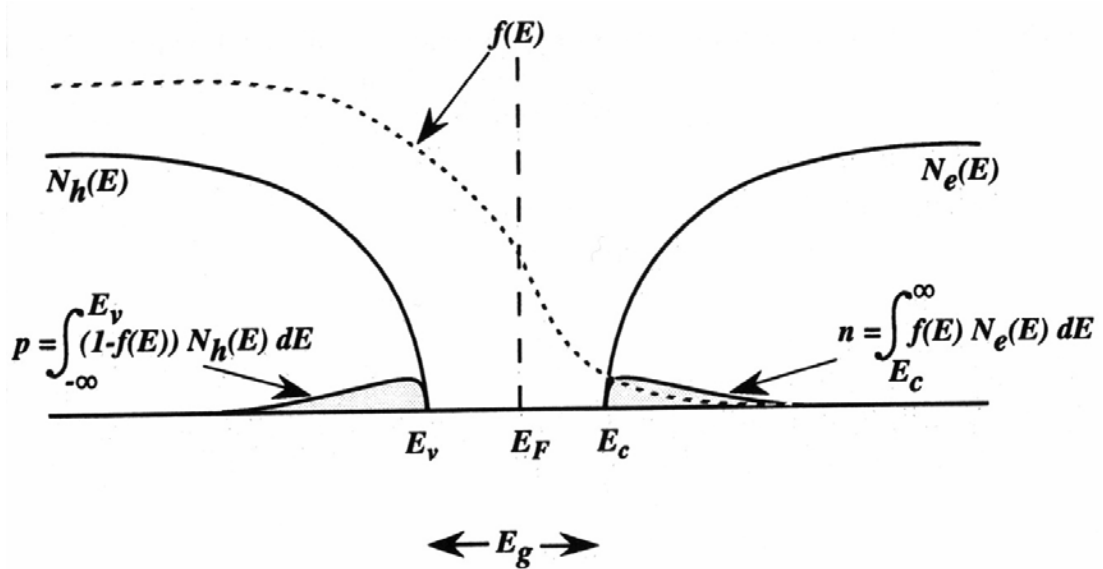


Fig .2.7 A schematic of the density of states of the conduction and valence band. N_e and N_h are the electron and hole density of states. The density of electron and holes are also shown [10].

Extrinsic semiconductors:

In order to control the electrical characteristics of the semiconductor devices, certain controlled amounts of impurities are purposely introduced into semiconductors and this can usually be done during the manufacturing stages of the semiconductor devices. There two possible charge carriers within the semiconductors which are namely negative (electron) or positive (holes). Which of them will be the dominant carrier is completely determined by the types of impurity elements introduced in the semiconductors. This type semiconductor is known as an extrinsic semiconductor [22].

By adding pentavalent impurities, into Si crystal, which have a valency of more than four, one can obtain a semiconductor such that its electron concentration is much larger than the hole concentration. This type of semiconductors is called as an *n-type* semiconductor. However, if one can add trivalent impurities to Si, such as

boron (B), which have a valency of less than four, there is an excess of holes over electrons. This kind is called as a *p-type* semiconductor [23].

Assuming that an element from the Vth column of periodic table such as As, which have five valence electrons, is substituted for one of the Si atoms within the crystal. Four out of these five electrons are shared with the four neighboring Si atoms. Thus when an As atom bonds with four Si atoms, it has eventually one electron left unbonded. Since this electron can not find a bond to go into, it is left orbiting around the As atom, as illustrated in below figure [22],

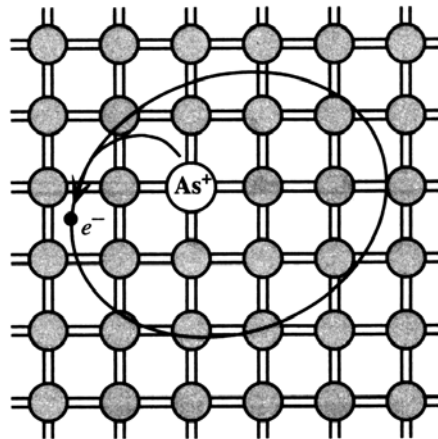


Fig.2.8 As-doped Si crystal. The fifth valance electron of As is orbiting around its side

As can easily give electrons to the conduction band and generate conduction electrons. These are known as donor atoms. Donor energy levels can be defined as the energy levels corresponding to the ground state binding energy of the loosely coupled electrons of the donor atoms. A semiconductor is then described as n-type if it is doped by donor atoms. Band structure and concentration of charge carriers for an n-type semiconductor are shown as follows [23]:

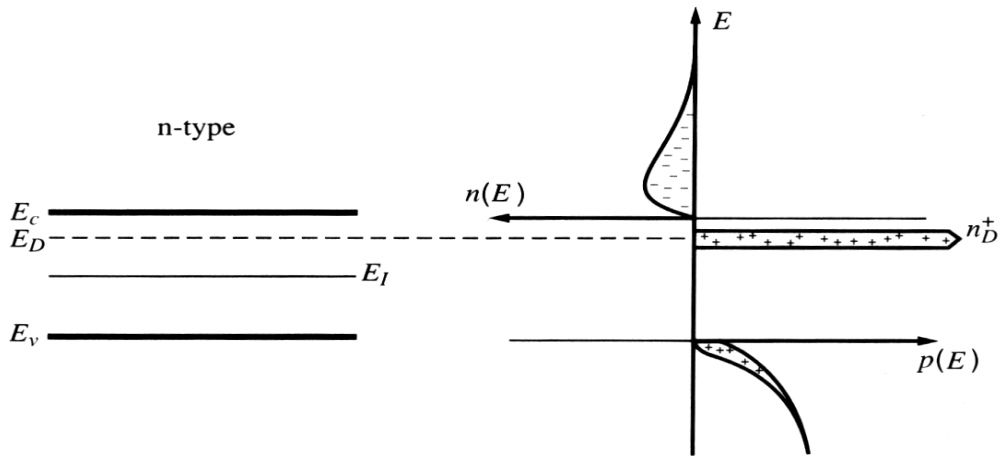


Fig. 2.9 Energy –band diagram and charge concentration in n-type semiconductors

When the impurity is an element from the IIIrd column, the situation becomes different since, unlike the previous case considered, a fourth valence electron to complete the electron pair binding process is absent and this makes the role of the impurity atom reversed. The nucleus of impurity atom is treated as a fixed negative charge and missing electron is replaced by a positive charge, circulating around this negative core.

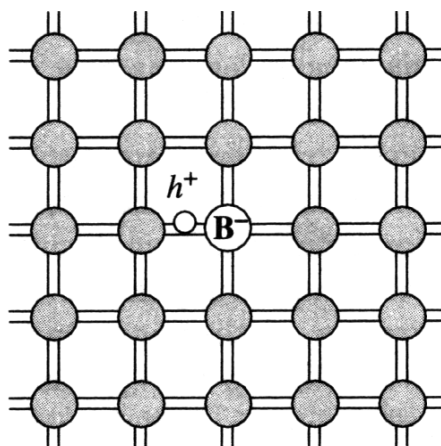


Fig. 2.10 B doped Si crystal. Substitution of Si leads to a missing electron which is indeed a hole (h^+) [22].

The addition of an impurity atom from IIIrd column leads to empty energy states above the top of the valence band so that valence electrons can move and thus generate additional holes in semiconductor at higher temperatures. The equivalent band diagram for this case is shown below [23];

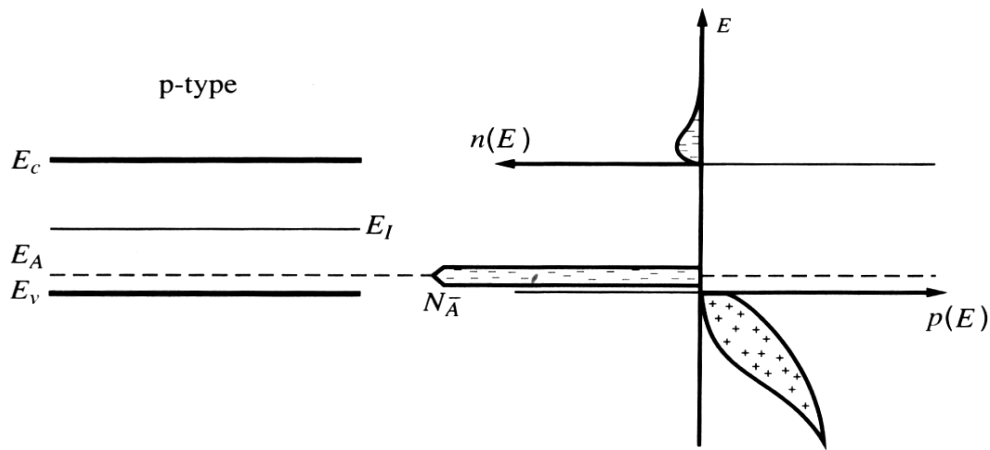


Fig.2.11 Energy –band diagram and charge concentration in p-type semiconductors.

The increase in temperature can easily make some of the electron at the top the valence band excited into these energy states. Then in the valence band empty states are formed and these are denoted as then equivalent to the generation of holes in the valence band. The resulting semiconductor is known as p-type since it has excess positive charge carriers introduced. The impurity atoms of the IIIrd column are known as *acceptor* since they simply accept electrons from the valence band. The corresponding energy level of the impurity atom is then called *acceptor energy level* whose band structure and concentration of charge carriers for a p-type semiconductor are shown in Fig. (2.10).

The carrier concentration in intrinsic and extrinsic semiconductors

Concentration of charge carriers can be calculated from the following integral equation. For electrons, the formula is

$$n = \int_{E_c}^{\infty} f(E) N_e(E) dE, \quad (2.9)$$

where E_c is the energy of conduction band, Fermi-Dirac function $f(E)$ and the electron density of states $N_e(E)$ in the conduction band are given

$$N_e(E) = \frac{1}{2\pi^2} \left(\frac{2m_e^*}{\hbar^2} \right)^{\frac{3}{2}} (E - E_C)^{\frac{1}{2}}, \quad (2.10)$$

$$f(E) = \frac{1}{1 + \exp\left(\frac{E - E_F}{k_B T}\right)}, \quad (2.11)$$

and a similar formula for holes can be written as

$$p = \int_{-\infty}^{E_v} [1 - f(E)] N_h(E) dE. \quad (2.12)$$

Then by putting Eqs. (2.10) and (2.11) into Eq. (2.9) we get an explicit expression for electrons as

$$n = \frac{1}{2\pi^2} \left(\frac{2m_e^*}{\hbar^2} \right)^{\frac{3}{2}} \int_{E_c}^{\infty} \frac{(E - E_C)^{\frac{1}{2}} dE}{\exp\left(\frac{E - E_F}{k_B T}\right) + 1}. \quad (2.13)$$

In order to put the carrier density expression into more compact form, let's define the following variables

$$\eta = \frac{E - E_C}{k_B T}, \quad \eta_F = \frac{E_F - E_C}{k_B T},$$

and we simply get

$$n = \frac{1}{2\pi^2} \left(\frac{2m^*}{\hbar^2} \right)^{\frac{3}{2}} \int_0^{\infty} \frac{\eta^{\frac{1}{2}} d\eta}{\exp(\eta - \eta_F) + 1}, \quad (2.14)$$

where the integral without the factor in front is called Fermi-Dirac integral,

$$F_{\frac{1}{2}}(\eta_F) = \int_0^{\infty} \frac{\eta^{\frac{1}{2}} d\eta}{\exp(\eta - \eta_F) + 1},$$

and further using the definition of the effective density of states at the

conduction bandedge $N_C = 2 \left(\frac{m_e^* k_B T}{2\pi \hbar^2} \right)^{\frac{3}{2}}$, we finally obtain

$$n = \frac{2}{\sqrt{\pi}} N_C F_{\frac{1}{2}}(\eta_F). \quad (2.15)$$

This expression can be solved numerically. However, a good approximation can be obtained by assuming Boltzman distribution instead of Fermi-Dirac distribution. In this case, the probability function for the electron can be approximated as

$$f(E) = \frac{1}{1 + \exp\left(\frac{(E - E_F)}{kT}\right)} \approx \exp\left(-\frac{(E - E_F)}{kT}\right).$$

This is indeed a good approximation for non-degenerate semiconductors. With this approach the above integral can be solved analytically and the electron concentration in Eq. (2.14) simply becomes

$$n = N_C \exp\left[\frac{(E_F - E_C)}{k_B T}\right]. \quad (2.16)$$

In a very similar way one can write the concentration of holes in the valance band from Eq. (2.12) within the above approximation as

$$p = N_V \exp\left[\frac{(E_V - E_F)}{k_B T}\right], \quad (2.17)$$

where $N_V = N_C (m_e^* \rightarrow m_h^*)$ is the effective density of states for the valance bandedge.

In intrinsic semiconductors the electron concentration is equal to the hole concentration since each electron in the conduction band leaves a hole in the valance band. If we multiply the electron and hole concentrations, we have

$$n p = 4 \left(\frac{k_B T}{2\pi\hbar^2}\right)^3 (m_e^* m_h^*)^{\frac{3}{2}} \exp\left(-\frac{E_g}{k_B T}\right), \quad (2.18)$$

and considering intrinsic case $n = p$, which can be denoted as n_i , we have from the square root of the equation above

$$n_i = 2 \left(\frac{k_B T}{2\pi\hbar^2}\right)^{\frac{3}{2}} (m_e^* m_h^*)^{\frac{3}{4}} \exp\left(-\frac{(E_C + E_V)}{2 k_B T}\right). \quad (2.19)$$

With the use of Eq. (2.19) Fermi energy in the intrinsic semiconductor E_{Fi} is then obtained

$$E_{Fi} = \frac{(E_C + E_V)}{2} + \frac{3}{4} k_B T \ln\left(\frac{m_h^*}{m_e^*}\right). \quad (2.20)$$

The Fermi level of an intrinsic material lies close to the midgap [10]. Energy bandgap diagram for intrinsic semiconductors can schematically be depicted as follows,

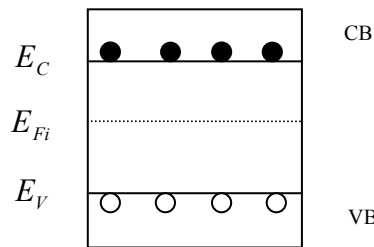


Fig. 2.12 Energy bandgap diagram for intrinsic semiconductors with Fermi level.

For the extrinsic semiconductors Fermi level is given in Fig. (2.13).

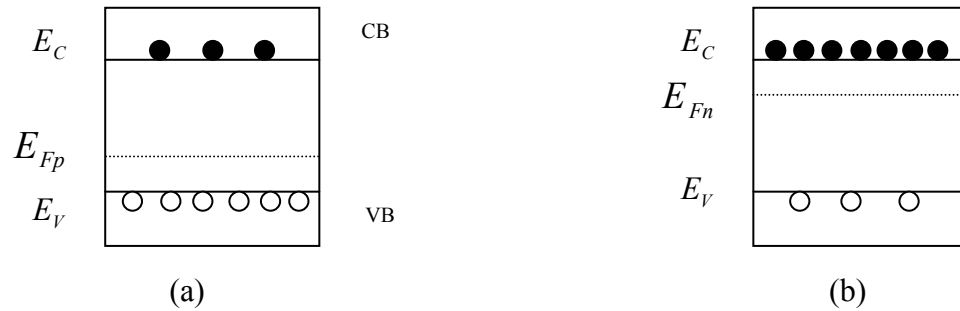


Fig.2.13 Energy bandgap diagram for extrinsic semiconductors with Fermi level. (a) for p-type, (b) for n-type.

2.1.6 Defects in semiconductors

It is well known that real crystals are never perfect: they always contain a considerable density of defects and imperfections that affect their physical, chemical, mechanical and electronic properties. Having defects in crystals, however, has very wide implications in various technological processes and phenomena such as annealing, precipitation, diffusion, sintering, oxidation and others. Defects can mostly be used as control parameter for getting desired characteristics in a system. Therefore, let us talk about the effects of imperfections or crystal defects on a few important properties of solids. The electrical behavior of semiconductors, for example, is largely controlled by imperfections inside the crystal and the development of the transistor and the entire field of solid state device technology has been originated from this fact.

In real semiconductors, one invariably has some defects that are introduced due to either thermodynamic considerations or the presence of the impurities during the crystal growth process. Defects, in general, in crystalline semiconductors can be characterized as i) point defects, ii) line defects, iii) planar defects, and iv) volume defects.

i) Point defects:

It is a highly localized defect that affects the periodicity of the crystal only in one or a few unit cells. Some possible kinds of point defects are represented in Fig. (2.13).

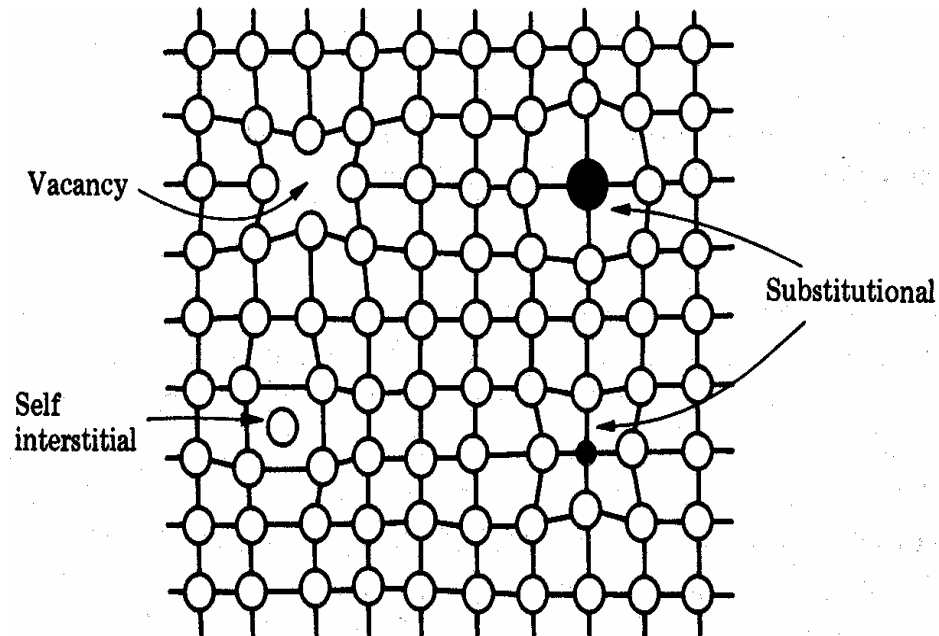


Fig .2.14 A schematic showing some important point defect in a crystal [10].

An impurity atom that occupies a normal lattice site is called a substitutional impurity atom and an impurity atom found in the interstice between matrix atoms is called an interstitial impurity atom. Whether a foreign atom will occupy a substitutional or interstitial site depends largely on the size of the atom relative to the size of the site. Small atoms have usually interstitial impurities, while larger atoms have usually substitutional impurities.

A vacancy is an atom site and it is usually occupied in the perfect crystal, from which an atom is missing. Often the term “vacancy” is used to denote a so-called Schottky defect, which is formed when an atom or an ion leaves a normal lattice site and repositions itself in a lattice site on the surface of the crystal. One

reason for that may be atomic rearrangement in an existing crystal at a high temperature, which happens when atomic mobility is high because of increased thermal vibrations. The process of crystallization, appearing as a result of local disturbances during the growth of new atomic planes on the crystal surface, might be taken another reason for vacancy formation. Vacancies are point defects of a size nearly equal to the size of the original (occupied) site; the energy of the formation of a vacancy is relatively low - usually less than 1 eV.

A vacancy pair defect formed by migration of a cation and an anion to the surface is usually called a Schottky imperfection, and a vacancy-interstitial pair defect is referred to as a Frenkel imperfection and it is formed by the result of the fact that an anion or cation has left its lattice position, which becomes a vacancy, and has moved to an interstitial position. These two types of imperfections are shown in Fig. (2.15).

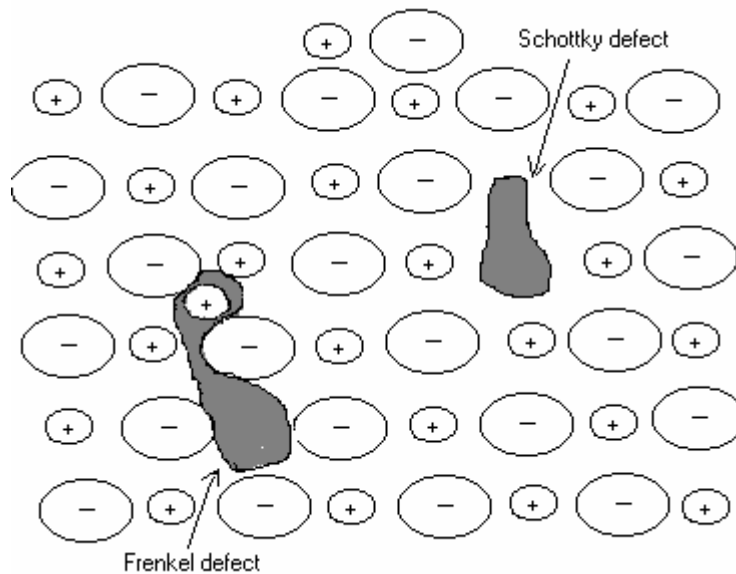


Fig. 2.15 Shottky and Frenkel defects.

Other point defects are interstitials in which an atom is sitting in a site in between the lattice points and impurity atoms which involve a wrong chemical species in the lattice. The point defects create a local disturbance in the crystal structure of semiconductors. The effect of this crystal disturbance can be divided into two categories:

i) The disturbance may create a potential profile which differs from the periodic potential only over one or a few unit cells. This potential is deep and localized and the defect is then called a deep level defect.

ii) Unlike the first case, the disturbance may create a long range potential disturbance which may extend over tens or more unit cells. Such defects are called shallow level defects.

ii) Line Defects or Dislocation:

In contrast to point defects, line defects (called dislocation) involve a large number of atomic sites that can be connected by a line. As shown in Fig. (2.16), dislocation is formed by inserting (removing) an extra half plane of atoms to (from) the crystal.

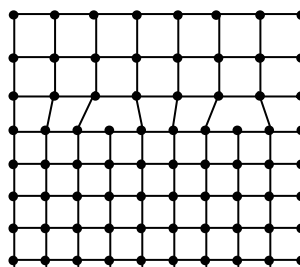


Fig. 2.16 Schematic presentation of a dislocation; the last row of atoms (dark) in the inserted fractional plane.

The importance of dislocations is readily demonstrated in the deformation of crystalline materials. The plane in which a dislocation moves through the lattice is

called a slip plane. With an applied shear stress the dislocation moves, atomic row by atomic row, and one part of the crystal is displaced relative to the other. When the dislocation has passed through the crystal, the portion of the crystal above the slip plane has shifted one atomic distance relative to the portion below the slip plane.

iii) Planar Defects and Volume Defects

The several different types of interfacial, or planar imperfections, in solids can be grouped into the following categories:

1. Interfaces between solids and gases, which are called free surfaces;
2. Interfaces between regions where there is a change in the electronic structure, but no change in the periodicity of atom arrangement, known as domain boundaries;
3. Interfaces between two crystals or grains of the same phase where there is an orientation difference in the atom arrangement across the interface; these interfaces are called grain boundaries;
4. Interfaces between different phases, called phase boundaries, where there is generally a change of chemical composition and atom arrangement across the interface.

Grain boundaries are peculiar to crystalline solids, while free surfaces, domain boundaries and phase boundaries are found in both crystalline and amorphous solids.

2.2 OPTICAL PROPERTIES OF SEMICONDUCTORS

2.2.1 Electrons in an electromagnetic field

To describe the interaction of an electron with the electric and magnetic fields of the electromagnetic field, the energy associated with this interaction is to be determined. Thus interaction Hamiltonian closely related to this energy is introduced and is used to describe the dynamics of the scattering electron.

The Hamiltonian for a particle of electric charge e ($e < 0$ for the electron) bound to a crystal potential $V(\vec{r})$ is

$$H_0 = \frac{\vec{p}^2}{2m} + V(\vec{r}). \quad (2.21)$$

When the electron is subject to electromagnetic field the classical Hamiltonian H_0 is modified as

$$H = \frac{1}{2m} \left(\vec{p} - \frac{e}{c} \vec{A} \right)^2 + e\phi + V(\vec{r}), \quad (2.22)$$

Where ϕ and \vec{A} are the scalar and vector potentials describing the electric and the magnetic fields.

Using the x-space representation of $\vec{p}, \frac{\hbar}{i} \vec{\nabla}$ the time dependent Schrödinger equation is

$$i\hbar \frac{\partial \psi}{\partial t} = H\psi, \quad (2.23)$$

where

$$H = -\frac{\hbar^2}{2m} \vec{\nabla}^2 + V(\vec{r}) + \frac{ie\hbar}{mc} \vec{A} \cdot \vec{\nabla} + \frac{ie\hbar}{2mc} (\vec{\nabla} \cdot \vec{A}) + \frac{e}{2mc^2} \vec{A}^2 + e\phi \quad (2.24)$$

By using the radiation gauge, $\vec{\nabla} \cdot \vec{A} = 0$ and $\phi = 0$, and assuming weak field approximation ($|\vec{A}|^2$ is negligible), the Hamiltonian becomes

$$H = H_0 + H', \quad (2.25)$$

where

$$H_0 = -\frac{\hbar^2}{2m} \vec{\nabla}^2 + V(\vec{r})$$

$$H' = -\frac{e}{mc} \vec{A} \cdot \vec{p}. \quad (2.26)$$

After defining the interaction Hamiltonian, the first order time dependent perturbation theory gives us the transition rate (that is, the transition probability per unit time) from the initial electron state $|i\rangle$ to a group of final state, represented by $[n]$, of the form

$$W(i \rightarrow [n]) = \frac{2\pi}{\hbar} \sum_n |V_{ni}|^2 \delta(E_n - E_i \mp \hbar\omega), \quad (2.27)$$

where $V_{ni} = \langle n | H' | i \rangle$ is the matrix element of the perturbation Hamiltonian and the minus sign in Dirac-delta function represents photon absorption and the positive one represents emission case. The Eq. (2.27) is known as Fermi's golden rule.

In order to compute the transition rates for either case, the matrix element V_{ni} needs to be evaluated. To this aim, let us work with a monochromatic field of the plane wave for

$$\vec{A} = 2A_0 \hat{\varepsilon} \cos\left(\frac{\omega}{c} \hat{n} \cdot \vec{r} - \omega t\right), \quad (2.28)$$

where $\hat{\varepsilon}$ and \hat{n} are the linear polarization and propagation direction and A_0 is the strength of the vector potential depending on photon number density. Note that the

gauge we used ($\vec{\nabla} \cdot \vec{A} = 0$) is obviously satisfied by this choice for \vec{A} , since $\hat{\epsilon}$ is perpendicular to \hat{n} . From the simple trigonometric relation $\cos \theta = \frac{1}{2}(e^{i\theta} + e^{-i\theta})$ we reexpress the vector potential as

$$\vec{A} = A_0 \hat{\epsilon} \left[e^{i\left(\frac{\omega}{c}\hat{n}\cdot\vec{r} - i\omega t\right)} + e^{-i\left(\frac{\omega}{c}\hat{n}\cdot\vec{r} + i\omega t\right)} \right], \quad (2.29)$$

where the absorption and the emission cases are more apparent. The term with $e^{-i\omega t}$ factor is responsible for absorption and the term with $e^{i\omega t}$ factor is responsible for emission. Then the interaction Hamiltonian from Eq. (2.26) becomes

$$\begin{aligned} H' &= -\frac{e}{mc} \vec{A} \cdot \vec{p} \\ &= -\frac{e}{mc} A_0 \hat{\epsilon} \cdot \vec{p} e^{\pm i\left(\frac{\omega}{c}\hat{n}\cdot\vec{r}\right)}, \end{aligned} \quad (2.30)$$

where + (-) sign refers to absorption (emission) case. The oscillatory time-dependent part, $e^{-i\omega t}$, is indeed represented in the argument of Dirac-delta function in Eq. (2.27).

Before dealing with the matrix element V_{ni} for the above perturbation H' , it is better to express the strength of the vector potential, A_0 , in terms of photon number density. From classical electromagnetic theory, the energy density of the electromagnetic wave is

$$u = \frac{1}{8\pi} (E^2 + B^2), \quad (2.31)$$

where $\vec{E} = -\frac{1}{c} \frac{\partial \vec{A}}{\partial t}$ and $\vec{B} = \vec{\nabla} \times \vec{A}$. By using Eq. (2.29) the electric and the magnetic fields become

$$\vec{E} = 2\frac{\omega}{c} A_0 \hat{\epsilon} \sin\left(\frac{\omega}{c} \hat{n} \cdot \vec{r} - \omega t\right),$$

$$\vec{B} = -2 \frac{\omega}{c} A_0 \hat{n} \times \hat{\varepsilon} \sin\left(\frac{\omega}{c} \hat{n} \cdot \vec{r} - \omega t\right). \quad (2.32)$$

Then from Eq. (2.32) and Eq. (2.31) we have

$$u = \frac{1}{2} \frac{1}{8\pi} \frac{8\omega^2}{c^2} |A_0|^2, \quad (2.33)$$

where we took time average of the fields. Also if there are n_p number of photons, the energy density for a volume V is

$$u = \frac{n_p \hbar \omega}{V} \quad (2.34)$$

Equating Eq. (2.33) and Eq. (2.34) we get

$$|A_0|^2 = \frac{2\pi\hbar}{\omega c^2 V} n_p \quad (2.35)$$

Now, let us turn back to the evaluation of the matrix element V_{ni}^a . If we first focus on the absorption case, the matrix element is

$$V_{ni}^a = \langle n | \left(\frac{-e}{mc} \right) A_0^a \hat{\varepsilon} \cdot \vec{p} e^{i\frac{\omega}{c} \hat{n} \cdot \vec{r}} | i \rangle, \quad (2.36)$$

where $A_0^a = \sqrt{\frac{2\pi\hbar}{\omega c^2 V} n_p}$.

The electric dipole approximation allows us to approximate the exponential term in Eq. (2.36) as 1 since the wavelength of the radiation field is far longer than the atomic dimension and thus $\left| \frac{\omega}{c} \vec{n} \cdot \vec{r} \right| \ll 1$ is directly obtained. The matrix elements for both cases are then

$$V_{ni}^a = \frac{-e}{mc} A_0^a \langle n | \hat{\varepsilon} \cdot \vec{p} | i \rangle,$$

$$V_{ni}^e = \frac{-e}{mc} A_0^e \langle n | \hat{\varepsilon} \cdot \vec{p} | i \rangle, \quad (2.37)$$

where $A_0^a = \sqrt{\frac{2\pi\hbar}{\omega c^2 V}}(n_p + 1)$, since there are $n_p + 1$ number of photons in the emission case which is denoted by the superscript “e”. By inserting the identity operator, $1 = \int d^3r |\vec{r}\rangle\langle\vec{r}|$, into the matrix elements we get

$$\begin{aligned} \langle n | \hat{\varepsilon} \cdot \vec{p} | i \rangle &= \int \int d^3r d^3r' \langle n | \vec{r} \rangle \langle \vec{r} | \hat{\varepsilon} \cdot \vec{p} | \vec{r}' \rangle \langle \vec{r}' | i \rangle \\ &= \int d^3r \psi_n^*(\vec{r}) \hat{\varepsilon} \cdot \vec{p} \psi_i(\vec{r}), \end{aligned} \quad (2.38)$$

where we have used $\langle \vec{r} | i \rangle \equiv \psi_i(\vec{r})$ and $\langle \vec{r} | \vec{r}' \rangle = \delta(\vec{r} - \vec{r}')$. Putting all these into the Eq. (2.27) we have

$$W^a(i \rightarrow [n]) = \frac{2\pi}{\hbar} \frac{e^2}{m^2 c^2} |A_0^a|^2 \sum \left| \int d^3r \psi_n^*(\vec{r}) \hat{\varepsilon} \cdot \vec{p} \psi_i(\vec{r}) \right|^2 \delta(E_n - E_i - \hbar\omega), \quad (2.39)$$

and a similar equation is for the emission case. In order to compute the transition rate we need to know the momentum matrix element. Therefore the transformation rate for absorption case can be written as

$$W^a(i \rightarrow [n]) = \frac{4\pi^2 \hbar n_p}{\hbar \omega c^2} \frac{e^2}{m^2 c^2} \sum_n |(\hat{\varepsilon} \cdot \vec{p})_{cv}|^2 \delta(E_n - E_i - \hbar\omega). \quad (2.40)$$

The sum over final states is zero except at resonance fixed by delta function. Thus this gives us the final state density of states of the form [10]

$$N_{cv}(\hbar\omega) = \frac{\sqrt{2} (m_r^*)^{3/2} (\hbar\omega - E_g)^{1/2}}{\pi^2 \hbar^3},$$

where m_r^* is the reduced mass of the electron-hole system and E_g is the parabolic band approximation. Finally the expression for transition rate in the case of

unpolarized light can be obtained by summing over all possible final polarization state and dividing over number of polarization states and then we get

$$W^a(i \rightarrow [n]) = \frac{4\pi^2 n_p e^2}{m^2 c^4 \omega} \frac{2}{3} p_{cv}^2 N_{cv}(\hbar\omega), \quad (2.41)$$

and a similar formula can be written for emission case. From this transition rate we can also compute absorption coefficient for interband transitions. The relation between them is

$$W^a = \alpha v n_p \quad (2.42)$$

where α is the absorption coefficient, v is the velocity of the wave in the medium, and n_p is the number of photons. This relation can be derived by using continuity equation for the photon density.

Having obtained the expression for absorption transition rate for direct gap interband transitions, we can further define absorption coefficient, which might be more useful than the rate at which photon is absorbed. To relate the absorption coefficient, α , to the absorption rate, W^a , one can consider the continuity equation for photon density and for photons traveling along x -direction it is given as in one-dimension

$$\frac{d}{dt} n_p = \frac{\partial n_p}{\partial t} + v \frac{\partial n_p}{\partial x} \quad (2.43)$$

where v is the velocity of the light in the medium, the first term, giving number of photons absorbed per unit time, represents the absorption rate, and the second one

represents the photon flux due to photon current. In the steady-state case $\left(\frac{\partial}{\partial t} = 0 \right)$

from the above relation we have

$$n_p(x) = n_0 e^{-\alpha x}, \quad (2.44)$$

where n_0 is the integration constant and α is called the absorption coefficient. Using

Eq. (2.43) and relation $\frac{\partial n_p}{\partial x} = -W n_p$ we get

$$\alpha = \frac{n_r}{c} \frac{1}{n_p} W, \quad (2.45)$$

where n_r is the index of refraction of the medium. Therefore the absorption coefficient for interband transitions becomes with the use of Eq. (2.41).

$$\alpha = \frac{4\sqrt{2}e^2(m_r)^3}{m^2 c^5 \hbar^3 \omega} \frac{2}{3} P_{cv}^2 (\hbar\omega - E_g)^{\frac{1}{2}} \quad (2.46)$$

where we consider the light unpolarized. From Eq. (2.45) we see that the absorption coefficient α starts as $\hbar\omega = E_g$, with zero value and initially increases as $(\hbar\omega - E_g)^{\frac{1}{2}}$.

As energy increases α behaves as $\frac{1}{\hbar\omega}$. Note that at higher energies parabolic band approximation is not valid. In order to evaluate α , we need to know p_{cv}^2 which can be obtained from a knowledge of the conduction band effective mass. The approximate relation between them can be written from detailed band structure calculations

$$\frac{1}{m^*} \cong \frac{1}{m} + \frac{2p_{cv}^2}{E_g}$$

As a final discussion of this section, we will talk about recombination time, τ_0 . To define τ_0 , the recombination rate of an electron with a hole at the same \vec{k} value (direct interband case) is needed. Note that in this we are dealing with emission rate and then the sum over final states in Eq. (2.40) turns into the sum over

all photon states into which such emission could occur. From Eqs. (2.37) and (2.39) we can write the emission rate as

$$W = \frac{2n}{\hbar} \frac{e^2}{m^2 c^2} \frac{2\pi\hbar}{\omega c^2} (n_p + 1) |\hat{\varepsilon} \vec{p}_{if}|^2 \rho_\varepsilon(\hbar\omega), \quad (2.47)$$

where ρ_a is the photon density of states for the polarization $\hat{\varepsilon}$ and the total photon density of states is given

$$\rho(\hbar\omega) = \frac{\omega^2}{\pi^2 \hbar v^2}. \quad (2.48)$$

Then if we consider the case $n_p = 0$ (vacuum state), the emission rate is called the spontaneous emission rate and we can define the electron-hole recombination time τ_0 as

$$\tau_0 = \frac{1}{W^e(n_p = 0)}. \quad (2.49)$$

The time τ_0 represents the time elapsed for an electron in a state k to recombine with a hole in a state with the same k value. If we consider unpolarized light case we get the expression for τ_0 as

$$\tau_0 = \left[\frac{4e^2}{3mc^2 \hbar^2 v^3} \left(\frac{2p_{cv}^2}{m} \right) \hbar\omega \right]^{-1}. \quad (2.50)$$

CHAPTER 3

PHOTOLUMINESCENCE SPECTROSCOPY

3.1 LUMINESCENCE SPECTROSCOPY

Luminescence spectroscopy is a powerful tool used for the characterization of semiconductors, especially those applicable for optoelectronic devices. It is a nondestructive technique that can yield information on fundamental properties of semiconductors. It is also sensitive to impurities and defects that affect materials quality and device performance. A brief introduction of luminescence spectroscopy and photoluminescence will be presented in this section.

Luminescence is the word for light emission after some energy was deposited in the material. There are several ways to excite sample to cause luminescence.

The most common method is Photoluminescence, which describes light emission stimulated by exposing the material to light - by necessity with a higher energy than the energy of the luminescence light. Photoluminescence is also called fluorescence if the emission happens less than about 1 μs after the excitation, and phosphorescence if it takes long times- up to hours and days - for the emission.

One possible way is to excite the sample by applying an external current, called as electroluminescence. Electroluminescence is particularly important in the

production of optoelectronic devices such as Light Emitting Diodes (LED), and LASERS.

Other ways are Cathodoluminescence, describes excitation by energy-rich electrons, chemoluminescence provides the necessary energy by chemical reactions and thermoluminescence describes production of radiation from sample by heating.

3.2 PHOTOLUMINESCENCE

Photoluminescence (PL) is a non-destructive optical technique used for the characterization, investigation, and detection of point defects or for measuring the band-gaps of materials. Photoluminescence involves the irradiation of the crystal to be characterized with photons of energy greater than the band-gap energy of that material. In the case of a crystal scintillator, the incident photons will create electron-hole pairs. When these electrons and holes recombine, this recombination energy will transform partly into non-radiative emission and partly into radiative emission.

Photoluminescence consists of impinging relatively high frequency ($h\nu > E_g$) light onto a material, exciting atomic electrons. Subsequent relaxation may result in the production of photons that are characteristic of the crystal or defect site that emits the light. The luminescent signals detected could result from the band to band recombination, intrinsic crystalline defects (growth defects), dopant impurities (introduced during growth or ion implantation), or other extrinsic defect levels (as a result of radiation or thermal effects). When bombarded with photons of energy greater than the bandgap of the material, an impurity energy level may emit characteristic photons via several different types of radiative recombination events, allowing the resultant PL spectra to be used to determine the specific type of

semiconductor defect. This interaction provides a highly sensitive, qualitative measurement of native and extrinsic impurity levels found within the material bandgap. We can briefly say photoluminescence process includes three main phases [24]:

1) Excitation: Electrons can absorb energy from external sources, such as lasers, arc-discharge lamps, and tungsten-halogen bulbs, and be promoted to higher energy levels. In this process electron-hole pairs are created.

2) Thermalization: Excited pairs relax towards quasi-thermal equilibrium distributions.

3) Recombination: The energy can subsequently be released, in the form of a lower energy photon, when the electron falls back to the original ground state. This process can occur radiatively or non-radiatively.

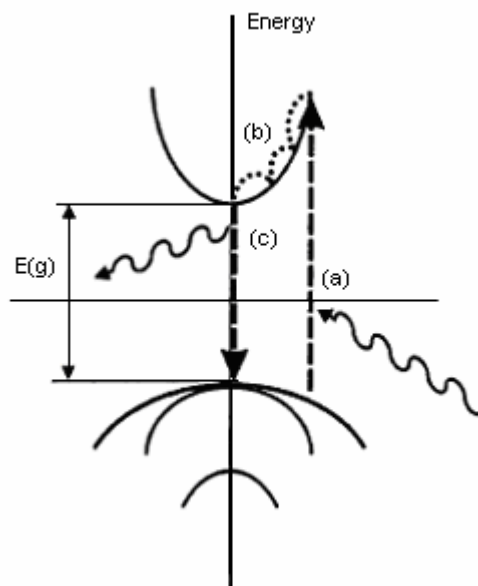


Fig.3.1 Photoluminescence schematic. (a) An electron absorbs a photon and is promoted from the valence band to the conduction band. (b) The electrons cools down to the bottom of the conduction band. (c) The electron recombines with the hole resulting in the emission of light with energy $h\nu$.

3.3 RECOMBINATION MECHANISMS

When a semiconductor absorbs a photon of energy greater than the bandgap, an electron is excited from the valence band into the conduction band leaving behind a hole. When the electron returns to its original state, it may do so through radiative (release of a photon) or non-radiative (no photon production) recombination. When the electron and hole recombine through radiative recombination, a photon is emitted and the energy of the emitted photon is dependent on the change in energy state of the electron-crystal system. Indirect bandgap semiconductor, photon emission requires the aid of a phonon (energy in the form of lattice vibrations) to conserve momentum within the lattice structure. With the introduction of impurities in semiconductor material discrete energy levels are formed within the semiconductor's forbidden energy gap. Shallow donor levels are defined as levels just below the conduction band, whereas, shallow acceptor levels are defined as levels just above the valence band. These donor or acceptor level traps can act as recombination centers for transitions within the bandgap. By studying the nature of these trap levels, information about the impurity or defect can be resolved. Figure 1 represents the energy band diagram of a semiconductor, illustrating the most common radiative and non-radiative transitions. (The conduction band (EC), occupied by free electrons, and the valence band (EV), occupied by free holes, are represented in addition to donor (ED) and acceptor (EA) trapping centers within the forbidden gap.) These transitions are band-to-band transition, free-to-bound transition, donor –acceptor pair transition, excitonic transition, auger transition.

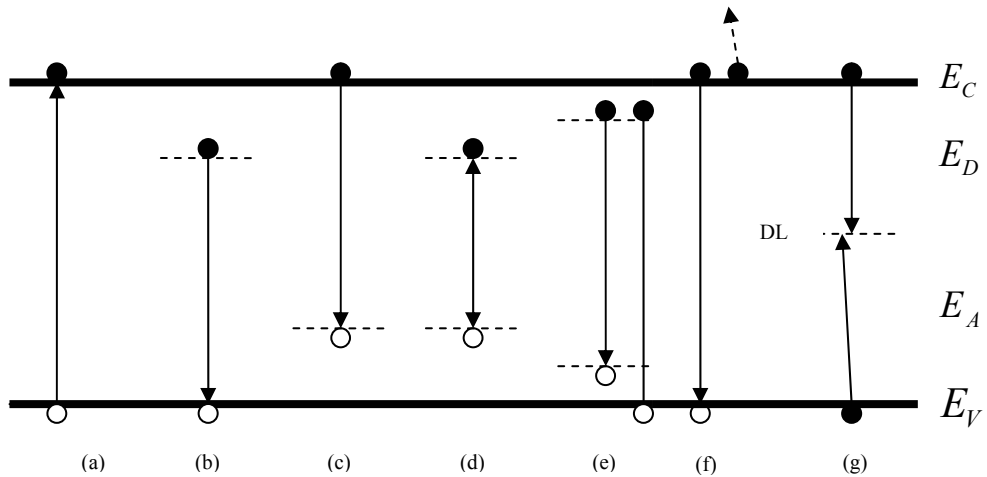


Fig.3.2 Most common radiative transition observable with photoluminescence and non-radiative transitions.

3.3.1 Band to Band Transition

The first transitions described here are radiative band-to-band or direct recombination [Fig.3.2 (a)], which dominate at room temperature and can be used to estimate the material bandgap energy (E_g). For indirect semiconductors a band-to-band recombination process is unlikely because the electrons at the bottom of the conduction band have a nonzero crystal momentum with respect to the holes at the top of the valence band.

Band -to-band transition contain the recombination of free electrons and free holes. This transition occurs when an electron falls from its conduction band state into the empty valence band state associated with the hole.. Band-to-band transition depends on the density of available electrons and holes and propability which is proportional to the absorption coefficient. So we can represent the recombination rate

$$U = R - G = \alpha(np - n_{ie}^2),$$

where, α is the recombination constant, n_{ie} is the effective intrinsic concentration, n electron and p hole concentration.

The energy, which is equal to the energy difference between the excited and ground states, released during the process usually produces a photon and emits light in a semiconductor having a direct band gap. It is given by the equation:

$$h\nu = E_f - E_i,$$

where E_f and E_i are, respectively, the final and initial state energies. In indirect semiconductors, band-to-band recombination occurs with phonon contribution and emitted photon energy is

$$h\nu = E_f - E_i \pm h\Omega,$$

Where $h\Omega$ is the energy of phonon.

3.3.2 Free to bound transition

At temperature for which $k_B T$ is greater than the ionization energy of shallow impurities, these impurities are ionized, hence band-to-band transition dominate. At sufficiently low temperatures the thermal energy of carriers becomes smaller than the ionization energy of the impurities in which case are frozen to the impurity. For example, in a p-type material containing N_A acceptors per unit volume, holes are trapped at the acceptor if $k_B T$ is smaller than E_A , where E_A is the ionization energy of the acceptor.

A free electrons can recombine radiatively (and sometimes non-radiatively) with the holes [Fig.3.2 (c)] trapped on acceptors or holes can recombine with the electrons trapped on the donors [Fig.3.2 (b)]. Such transition involving free carrier

(electron) and a charge (hole) bound to an impurity, are known as free-to-bound transition. The emitted photon energy is given by

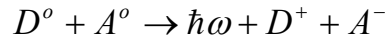
$$h\nu = E_g - E_A,$$

where E_A is the acceptor shallow binding energy. The equation can be written for the transition, donor to valance band with the energy E_D .

If an electron is captured at a donor site, however, it has a high probability at room temperature of being re-emitted into the conduction band before completing the remaining steps of the recombination process. A similar statement can be made for holes captured at acceptor sites. For this reason sites may be likened to extremely inefficient R-G centers, and the probability of recombination occurring via shallow levels is usually quite low at room temperature. It should be noted, nevertheless, that the largest energy step in shallow-level recombination is typically radiative and that the probability of observing shallow-level process increases with decreasing system temperature.

3.3.3 Donor-Acceptor Pair Transition

When both donor and acceptor impurities are present in semiconductors, coulomb interaction between the donors and acceptors modifies the binding energy in such a way that the transition energy is distance dependent. The DAP (donor acceptor pair) complex consists of four point charges like an exciton neutral impurity complex (bound exciton). The donor ion D^+ and the acceptor ion A^- are immobile point charges while the remaining two charges, an electron and a hole, are mobile. [Fig.3.2 (d)] shows the usual situation for pair recombination. This process represented by the reaction



The recombination energy of a donor acceptor pair given by

$$E(r) = E_g - (E_D + E_A) + \frac{e^2}{\epsilon r},$$

where E_g is the bandgap energy, E_D and E_A are the binding energy of the donor and the acceptor and the last term is the coulombing interaction of the donor–acceptor pair separated by r .

3.3.4 Exciton Transitions

Free Exciton:

Excitonic recombination, can occur following the generation of an electron-hole pair (Fig.1.e). Coulombing attraction leads to the formation of an excited state in which an electron and the hole remain bound to each other in a hydrogen-like state, referred to as a free exciton [25].

The energy of the emitted photon is

$$h\nu = E_g - E_X$$

where E_g is the bandgap energy of the semiconductor and E_X is the Coulomb energy of the exciton.

Bound Exciton (Exciton-Impurity Interaction):

In reality, many semiconductor materials contain small amounts of natural defects or impurities forming neutral donors and acceptors. Optically generated free excitons can interact with those impurities and may become captured by them. They are then called donor-bound or acceptor-bound excitons depending on whether the impurity that the exciton is attached to is a donor or an acceptor.

Energy is the fundamental criterion that determines whether or not a free exciton can be trapped at an impurity. If the total energy of the system is reduced when the free exciton is in the vicinity of the impurity, then it is energetically favorable for the exciton to remain near the defect the exciton becomes bound to the impurity via van der Waals interaction [26] .

These bound exciton can be considered as analog to the hydrogen molecules H_2 except for different binding energies. Bound exciton have much smaller binding energies (usually a few milielectronvolts) because the hole mass is much smaller than that of the proton and in a medium coulomb interaction is lowered by the square of the dielectric constant. The common nomenclature is (D^o, X) and (A^o, X) for neutral-donor bound and neutral-acceptor bound excitons. A photon being emitted following a bound exciton annihilation has the energy

$$h\nu = E_g - E_X - E_B ,$$

where E_B is the binding energy of the exciton to the defect.

Exciton –Phonon Interaction(Phonon assisted Exciton):

Momentum conservation rules required that only those free excitons can recombine radiatively which have the same k-vector as the out going photon. Since the photon momentum is small compared to the momentum of excitons, only excitons with virtually no kinetic energy ($K=0$) are allowed to recombine. However, this condition does not prevent the excitons from having kinetic energy. Recombination of free excitons with momentum other than the outgoing light can occur through phonon participation. Phonons provide the necessary momentum to satisfy the momentum conservation law and thereby reduce restriction on the free

exciton momentum allowing of excitons finite K to annihilate. For one-phonon emission the momentum, and energy conservation law can be expressed as

$$K = k + q_{ph}$$

$$h\nu = E_X(K) - h\nu_{ph},$$

where the subscript “ph” refers to the phonons and $E_X(K)$ is the total energy of free exciton.

3.4 DEPENDENCE OF PHOTOLUMINESCENCE ON LASER EXCITATION POWER

The variation of photoluminescence intensity, which depends on the power of the excitation light source can be used to identify the underlying recombination process [27]. This is since that the power of the excitation light source is varying. The general conclusion from the refs. [28,29] is that the luminescence intensity I of the near bandedge photoluminescence emission lines is proportional to L^k , which can be expressed as

$$I \propto L^k,$$

where L is the power of the exciting laser radiation and $1 < k < 2$ for exciton like transition and $k < 1$ for free to bound and donor to acceptor pair ($D^0 A^0$) transition.

In order to explain most of the features of near bandedge photoluminescence emission lines, observed by experiments, [28] *et.al* proposed a model to predict the excitation power dependence of these lines which include free-exciton, bound-exciton, free-to-bound, and donor-acceptor recombination processes. Within framework of their model, the set of rate equations can be used to describe each of

the above recombination mechanisms. By assuming that the electron concentration, n , in the conduction band and the hole concentration, p , in the valence band are equal to each other, and further ignoring thermal dissociation of free and bound excitons, the following coupled differential equations are obtained

$$\frac{dn}{dt} = iL - an^2 - gn(N_D - N_{D^0}) - enN_{A^0} \quad (3.1)$$

$$\frac{dn_{FE}}{dt} = an^2 + jL - \left(\frac{1}{\tau_{FE}} + \frac{1}{\tau_{FE}^{nr}} \right) n_{FE} - bn_{FE}N_{D^0} - cn_{FE}N_{A^0} \quad (3.2)$$

$$\frac{dn_{DX}}{dt} = bn_{FE}N_{D^0} - \left(\frac{1}{\tau_{DX}} + \frac{1}{\tau_{DX}^{nr}} \right) n_{DX} \quad (3.3)$$

$$\frac{dn_{AX}}{dt} = cn_{FE}N_{A^0} - \left(\frac{1}{\tau_{AX}} + \frac{1}{\tau_{AX}^{nr}} \right) n_{AX} \quad (3.4)$$

$$\begin{aligned} \frac{dn_{A^0}}{dt} = & h(N_A - N_{A^0})n + i(N_A - N_{A^0})L - cn_{FE}N_{A^0} \\ & + \left(\frac{1}{\tau_{AX}} + \frac{1}{\tau_{AX}^{nr}} \right) n_{AX} - dN_{D^0}N_{A^0} \end{aligned} \quad (3.5)$$

$$\begin{aligned} \frac{dn_{D^0}}{dt} = & g(N_D - N_{D^0})n + kN_{D^0}L - bn_{FE}N_{D^0} \\ & + \left(\frac{1}{\tau_{DX}} + \frac{1}{\tau_{DX}^{nr}} \right) n_{DX} - dN_{D^0}N_{A^0} - fN_{D^0}n \end{aligned} \quad (3.6)$$

In equation (1) - (6) N_D and N_A concentration of donors and acceptors, N_{D^0} and N_{A^0} are the concentration of neutral donors and acceptors, τ_{FE} and τ_{FE}^{nr} are the radiative and nonradiative lifetimes of donor free excitons, and τ_{DX}^{nr} , τ_{DX} , τ_{AX} , τ_{AX}^{nr} are clear now on. n_{FE} , n_{DX} and n_{AX} are the concentrations of free and bound excitons, respectively, and L is the laser intensity. The

coefficients a, b, \dots, l are the transition rates of certain recombination processes as explained in the beginning of this chapter. When we consider the steady state form of the above differential equations, we are left with a set of algebraic equations and the luminescence intensities of free and bound excitons, denoted as $I_{FE}, I_{D^0X}, I_{A^0X}$, are deduced through the Eqs. (3.2), (3.3) and (3.4) of the forms

$$I_{FE} = \frac{n_{FE}}{\tau_{FE}} = \frac{\beta}{\tau_{FE}} n^2, \quad (3.7)$$

$$I_{D^0X} = \frac{n_{DX}}{\tau_{DX}} = \frac{bN_{D^0}\beta}{1 + \frac{\tau_{DX}}{\tau_{DX}^{nr}}} n^2,$$

$$I_{A^0X} = \frac{n_{AX}}{\tau_{AX}} = \frac{bN_{A^0}\beta}{1 + \frac{\tau_{AX}}{\tau_{AX}^{nr}}} n^2, \quad (3.8)$$

where

$$\beta = \frac{a}{\left(\frac{1}{\tau_{FE}} + \frac{1}{\tau_{FE}^{nr}}\right) + bN_{D^0} + cN_{A^0}} \quad (3.9)$$

When N_{D^0} and N_{A^0} are constant the Eqs. (3.1)-(3.4) is enough and Eq. (3.1) allows us to express the electron concentration n in as a function of L in the steady state case of the form

$$n = \frac{i}{eN_{A^0} + g(N_D - N_{D^0})} L \quad (3.10)$$

Then eliminating all n terms from the Eqs. (3.7), (3.8) and (3.9), they read as

$$I_{FE} = \frac{\beta}{\tau_{FE}} \frac{i^2}{[eN_{A^0} + g(N_D - N_{D^0})]^2} L^2$$

$$\begin{aligned}
I_{D^0X} &= \frac{bN_{D^0}\beta}{1 + \frac{\tau_{DX}}{\tau_{DX}^{nr}}} \frac{i^2}{[eN_{A^0} + g(N_D - N_{D^0})]^2} L^2 \\
I_{A^0X} &= \frac{cN_{A^0}\beta}{1 + \frac{\tau_{AX}}{\tau_{AX}^{nr}}} \frac{i^2}{[eN_{A^0} + g(N_D - N_{D^0})]^2} L^2
\end{aligned} \tag{3.11}$$

Where the dependence for the free-exciton and bound-exciton intensities on L is quadratic. Note that for the free-to-bound transitions there is a linear relationship between the free-to-bound transition intensities and L , which can be deduced by assuming that the intensity of free-to-donor (acceptor) transitions are proportional product of both the electron concentration and the concentration of donor (acceptor).

3.5 TEMPERATURE DEPENDENCE OF PHOTOLUMINESCENCE

In this section we want to briefly discuss the effect of the temperature both on the fundamental gap energy, E_g , and on the variation of emission intensity. As we noted before the temperature dependency of E_g can be in generally described by the empirical formula in Eq. (2.3) as of the form

$$E_g(T) = E_g(0) - \frac{\alpha T^2}{T + \beta}, \tag{2.3}$$

where $E_g(0)$ is the bandgap energy at 0 K, α and β are constants. Furthermore, variation in E_g in semiconductors is usually explained by two factors. The first factor is electron-phonon interaction, and the second one is the thermal expansion of crystal lattice. The temperature dependent interaction potential describing electron-phonon couplings can indeed give the major contribution to shift in relative position of the conduction and the valance bands. These interaction leads to a decrease in E_g

as the temperature increasing. This behavior can be understood from the above empirical formula for high temperature values. As T becomes high, the second term in the Eq. (2.3) behaves as $-\alpha T$, resulting in a decrease in E_g with respect to its value at 0 K.

The second factor may lead to either decrease or increase in E_g with temperature. However, it has smaller contributions to $E_g(T)$ than that came from electron-phonon interaction. Theoretical calculations show that the effect is linear with T at high temperature unlike the case at lower temperature where α and β have non-linear T dependency. This means that at low T the dependency is automatically nonlinear.

The temperature dependence of photoluminescence is often used to probe the energy levels involved in certain transitions. In order to achieve this aim, we need to express the variation of emission intensity with temperature which can be formulated as

$$I(T) = \frac{I(0)}{1 + A \exp\left(\frac{-E_a}{kT}\right)} \quad (3.12)$$

where A is a constant, k is Boltzmann's constant, and E_a is the thermal activation energy of the transition. For temperature large enough that the following condition is satisfied,

$$A \exp\left(\frac{-E_a}{kT}\right) \gg 1,$$

the Eq. (3.12) takes the form

$$I(T) \propto \exp\left(\frac{-E_a}{kT}\right).$$

Therefore, the value of E_a can easily be deduced from the slope of the plot of $\text{Log}(I)$ versus $1/kT$. The significance of E_a comes from the fact that with the use of it one can determine the energy levels inside the bandgap of semiconductor, which is the ultimate point to be reached.

3.6 SETUP OF PL

The basic equipment setup needed to perform conventional photoluminescence consists of three main parts: (1) a light source to provide above- or below-band-gap excitation; (2) a dewar to maintain the samples at low temperatures while allowing optical access to the sample surface; and (3) a detection system to collect and analyze the photons which are emitted from the sample.

A diagram describing the experimental PL set-up is presented in Fig (2.4.3). Each sample was mounted to a cold finger and placed into a liquid helium-cooled cryostat that was cooled to the sample temperature variation from 15 K to 300K. The temperature of the sample was monitored using a Lake Shore 330 Temperature controller within an accuracy of ± 0.5 K. The measured luminescence was generated by 337.1 nm, N_2 Laser system operating at average power of 7 mW. The luminescence collection and detection equipments consists a pair of lenses, mirror, monochromator, Charge-Coupling-Devices (CCD), and computer (PC). The excitation pulsed was directed to the sample using mirror, Oriel 17960. The luminescence emitted was focused by two convex lenses onto the entrance slit of Oriel model 77700a *MS257TM* monochromator and spectrograph. The signal was spectrally resolved with monochromator. The monochromator is equipped four (4) grating with 1200 lines/mm- blaze wavelength 350 nm, 300 lines/mm-blaze.

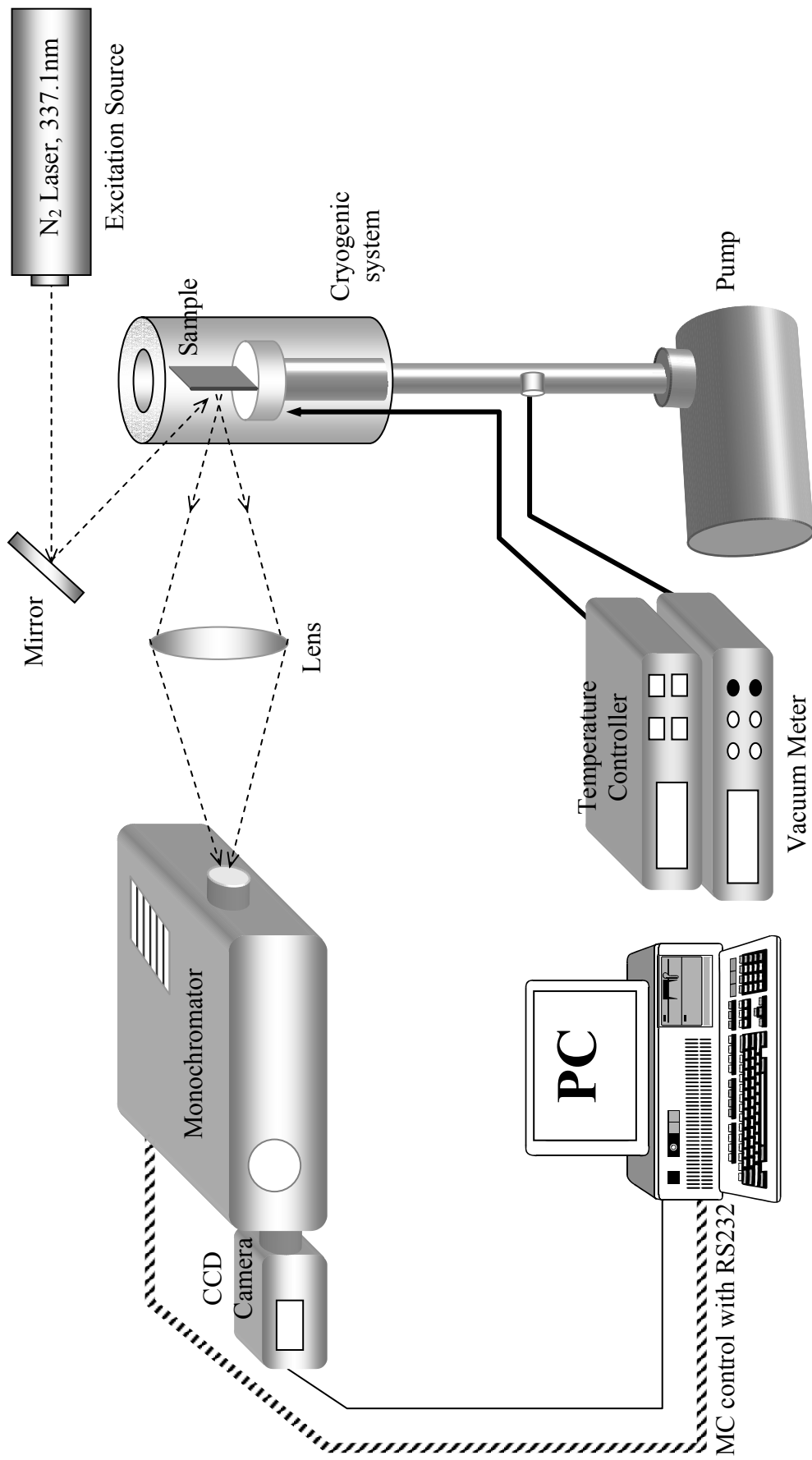


Fig.3.3 The schematic representation of Photoluminescence set-up.

wavelength 400 nm, 150 lines/mm-blaze wavelength 4000 nm, 75 lines/mm-blaze wavelength 8000 nm. The model 77721 fixed slit housing was used with mounting of Oriel 1.5 inch (47mm) series. The slit height is 15 mm. The micrometer drive is metric and a $10\mu\text{m}$ movement of the micrometer spindle corresponds to $10\mu\text{m}$ change in slit width. Slit width usually sets a limit on the resolution of spectrum, in our cases it was 1 mm for GaSe, and 35 micron for CdS. The control of the monochromator was done through RS232 port of the computer by using programs written in LABVIEW. The Hamamatsu C7041 (S7031-1008 series with 1044×256 number of pixel) multichannel detector was used to detect the PL signals. The C7041 are high sensitivity multichannel detector heads developed for use with back-timed FFT-CCD area image sensors that offer high UV sensitivity and quantum efficiency and it is designed for a thermoelectrically cooled CCD image sensor for detection at even lower light levels. The spectra were recorded using a conventional PC equipped with a SCSI card for the CCD camera. Data acquisition was performed by using a special computer program provided by the manufacturer.

3.7 EXPERIMENTAL TECHNIQUES USED IN PHOTOLUMINESCENCE EXPERIMENTS

In the experiments all samples were prepared almost parallel to the crystal layer. The samples were loaded onto the cold-finger holder, represented Fig. (3.4), of the closed-cycle cryostat. The PL was observed from the laser-illuminated face of the samples. All PL spectra were recorded when the system temperature was stabilize around desired value, which usually requires approximately 15-20 minutes. Some PL

spectra have been analyzed by using fitting procedure to deconvolve the complex bands. To do this, we used the Originpro 7.0 peak fit program.

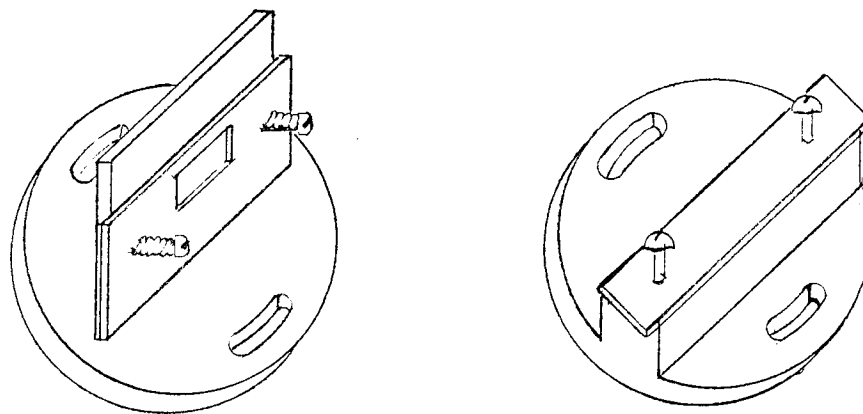


Fig.3.4 Holders

CHAPTER 4

PHOTOLUMINESCENCE PROPERTIES OF COMPOUND

SEMICONDUCTORS CdS AND GaSe

4.1 INTRODUCTION

Light emission from compound semiconductors has been an important phenomenon due to its technological applications. Most of the optoelectronic components such as light emitter or photodetectors are being fabricated on compound semiconductors having a direct bandgap with a high emission probability. Light emission from a semiconductor is a result of transition of a charge carrier from a higher energy state to a lower state. Usually an electron in the conduction band makes a transition from conduction band to valence band and recombines with a hole. This transition takes place effectively only when the semiconductor has a direct bandgap. Photoluminescence properties of compound semiconductors have thus been subject of many investigations. Understanding PL spectra of semiconductors are not always straightforward even for compound semiconductors with relatively simple band structure. Difficulties arise from the fact that the light emission can result from various sources that might not be easily resolved. In this work we have studied PL properties of compound semiconductors CdS and GaSe which exhibits interesting features.

CdS is a direct bandgap material and has been of interest due to its high efficiency in the solar cells. It is also known as an efficient light emitter of green light resulting from the band-to-band transition. Recently, it has attracted a great deal of attention for the production of nanocrystals for biomedical applications. CdS has a bandgap of 2.42 eV which corresponds to a light wavelength of 510 nm at 300 K. It is a good material to study the photoluminescence properties.

GaSe is an interesting compound semiconductor with a layer structure. It has several different phases with different electro-optical properties. Photoluminescence properties of GaSe crystal show a series of interesting and complicated features. A series of PL peaks with energies very close to the bandgap are usually observed. Understanding these features is still a challenging scientific task. One of the reasons that make the PL properties of GaSe complicated is that it has both direct and indirect conduction band edges at closely spaced energy positions in the Brillouin zone. Some researchers have attributed the observed multiple PL peaks to the presence of two conduction band edge minimum. Also, the optical anisotropy that exists in both absorption and emission spectra of GaSe makes the PL analysis even more complicated. Absorption/emission spectra along the direction of crystal axis which is perpendicular to the plane of the crystal layers has been found to be different than that observed in the parallel direction. This behaviour has been explained by the selection rules resulted from the anisotropy of the crystal. In this work, we have studied the PL properties of GaSe crystal grown by Bridgman technique in the Crystal Growth Lab. of Physics Department. The dependence of the PL peaks on temperature and on the polarization has brought about new evidences on the band structure and anisotropy of GaSe crystal.

4.2 PHOTOLUMINESCENCE PROPERTIES OF CdS

The PL spectrum of a commercially available CdS crystal at $T = 20$ K is shown in Fig.4.1. A series of PL peaks are identified and labeled as PL1, PL2, PL3, PL4, PL5, PL6, and PL7. The strongest peak (PL1) observed at 490 nm (2.53 eV) results from the emission from the free exciton located below the conduction bandedge. Taking the free exciton binding energy as 0.121 meV, we find the bandgap energy of CdS to be 2.651 eV at 20 K. This value is in agreement with the reported values of CdS crystal. Four small green PL peaks seen in the low energy side of the main FE peak were observable below 70 K. The origin of these peaks is discussed below. A broad red peak (PL6) centered around 696 nm is visible in all accessible temperatures. Another peak (PL7) whose peak energy located around 449nm (2.76 eV) is larger than the bandgap value becomes visible in temperature range of 130 K to 20 K.

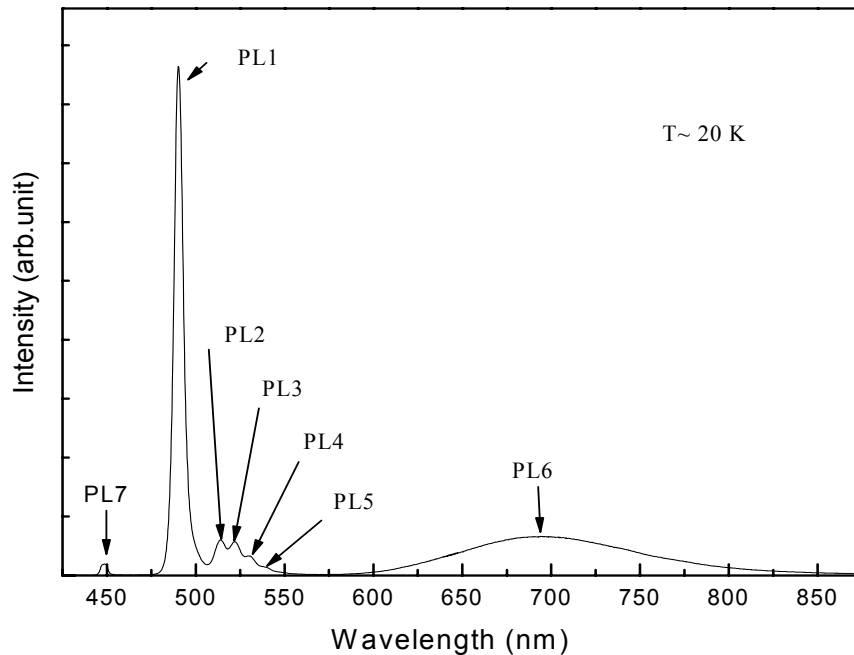


Fig.4.1 Photoluminescence spectrum of CdS at $T \sim 20$ K

Fig.4.2, Fig.4.3, and Fig.4.4 show the temperature dependence of the photoluminescence spectra of CdS in the range of 20-300 K. As can be seen in Fig.4.2, at room temperature this sample exhibits two broad emission bands at green (2.53eV) and red (1.78eV) in agreement with previously reported results [31]. As the temperature decreases from 300 to 20 K, the luminescence spectrum changes drastically. Four peaks located in the range of 2.3-2.53 eV emerge in temperature range from 70K to 20 K. The variation of these four peaks with temperature is shown in Fig.4.3. The broad red peak shown in Fig.4.4 is visible only in the temperature range of 22-80K.

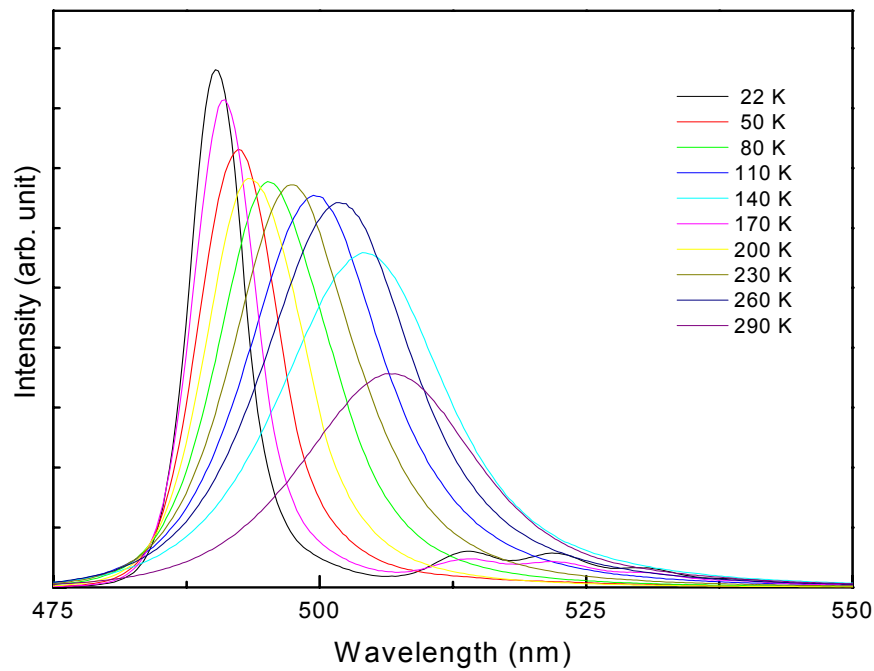


Fig.4.2 PL spectra of green band of CdS as a function of temperature.

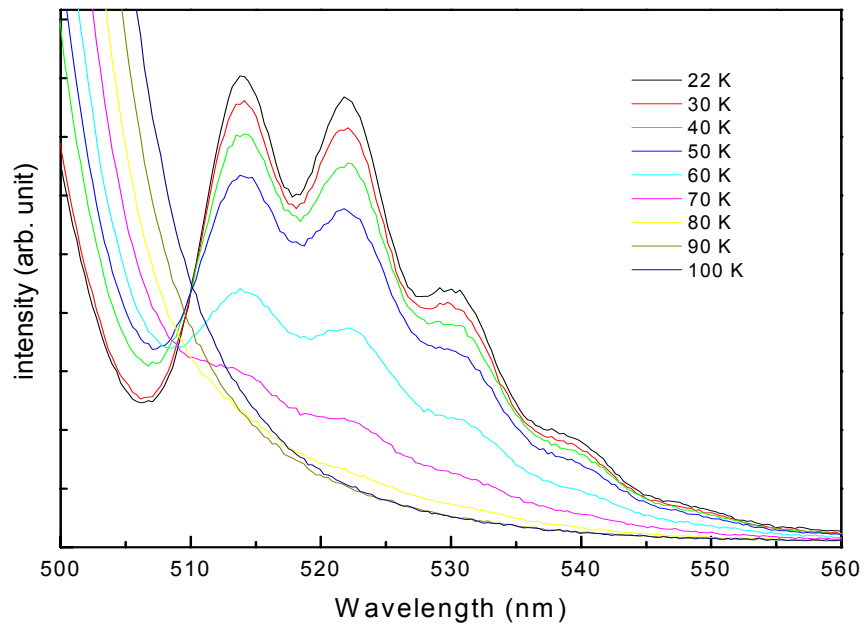


Fig.4.3 PL spectra of the near bandedge transitions of CdS as a function of temperature

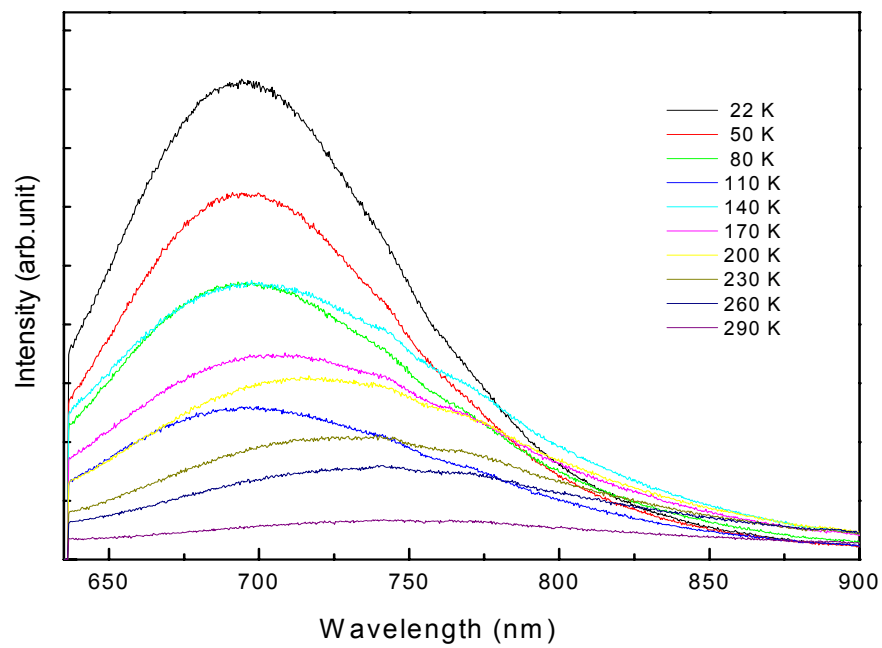


Fig.4.4 PL spectra of red band for CdS as a function of temperature.

The PL spectra of CdS at low temperatures exhibit usually complicated structure with many emission peaks which are attributed to the transitions involving both band edge states and localized states of donor and acceptor centers [32]. In the light of these findings reported previously, the PL emission shown in Fig.4.1 and 4.2 can be explained by a model described schematically in Fig. 4.5 As mentioned above the main green peak located at 490 nm (2.53 eV) is a result of free exciton emission across the bandgap of CdS. Four small peak in the low energy side of the FE peak resulted from the emissions involving localized states. The origin of PL2 peak with the energy of 2.41 eV is likely to be bound exciton [33] with a binding energy of 0.0079 eV.

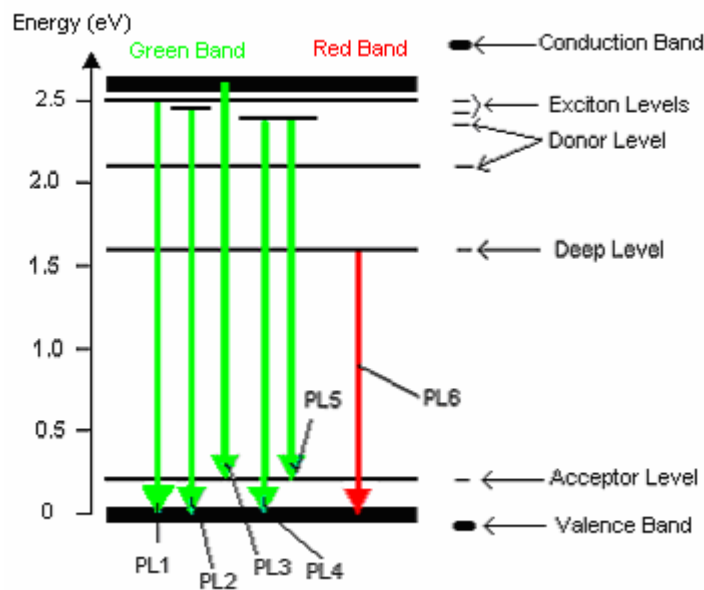


Fig.4.5 Optical transition in CdS crystal.

The third peak located at 2.37 eV is assumed to be a transition from the conduction band to the acceptor state and the peak PL4 at 2.33 eV is a transition from a donor level to the valence band. The last element of the green band, PL5 at

2.30 eV is likely to result from the donor-acceptor transition. The origin of the donor and acceptor states were discussed in the reports published previously [34]. Even though there might be conflicting results in the literature and the presented evidences are not convincing enough, some self consisted explanations have been generally accepted. Donor levels in CdS were attributed to the S vacancies in the CdS crystals [35, 36, 37]. The acceptor states were attributed to S interstitials [38]. Both of these descriptions were supported by other experimental evidences [39]. The broad red band with the peak position at 696 nm was observed by many groups working on CdS. The origin of this emission is believed to be the transition through the deep level created by S vacancies. The logarithmic variation of the peak intensity of the red emission with $1/kT$ is plotted in Fig.4.6. The slope of the straight part of this plot, which is the activation energy of this emission, is found to be 0.121 eV. This value is close to what was obtained in a similar experiment [40]. We can conclude that there exists another donor level located 0.121 eV below the conduction band edge as illustrated in Fig. (4.5). The red emission is then found to be a multi step transition process: in the first step electrons drop to the first donor level located 0.121 eV below the conduction band edge, and then make a transition to the second deep donor level at 1.78 eV above the valence band. Finally they fall into the valence band giving the red emission.

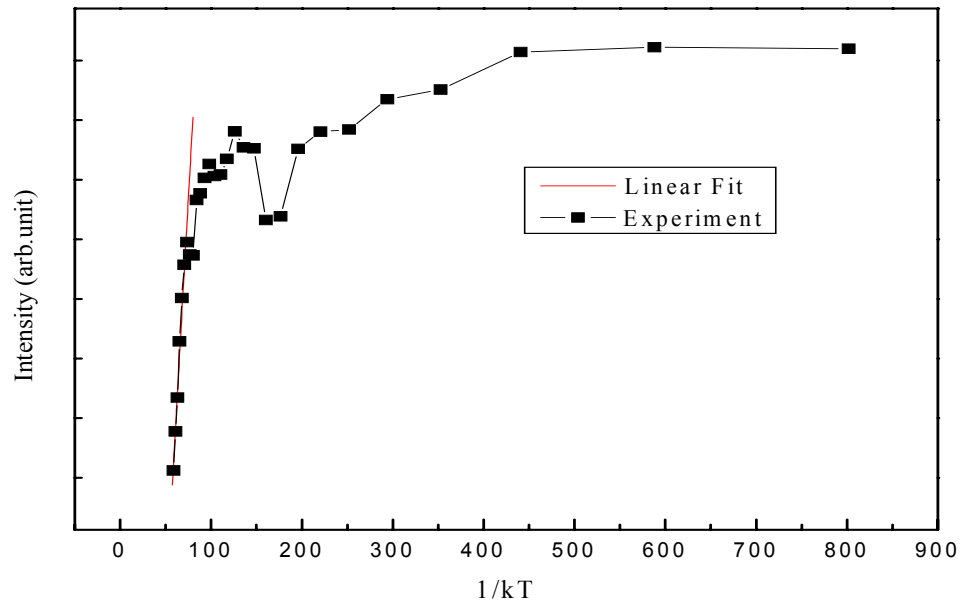


Fig.4.6 Temperature dependences of red band CdS PL intensity at the emission band maxima.

4.3 PL SPECTRUM AND BAND STRUCTURE OF GaSe

GaSe is a highly anisotropic semiconductor which consists of layers of covalently bounded Ga and Se atoms. The layers are bound by weak Van der Waals forces. The difference in the stacking sequence of the Ga and Se atoms leads to different polytypes of GaSe identified as β , γ , and ϵ types. These different polytypes have slightly different optical properties. It has been suggested that different polytypes might exist in the same sample [41].

The electronic band structure of GaSe shows the existence of a low lying indirect gap in GaSe. The indirect minimum of the conduction band at the M point of the Brillouin zone is lower than the direct bandgap located at Γ point of the zone. It was found that the indirect band edge is located 25 meV below the direct band edge. Thus one might argue that GaSe is an indirect bandgap material. However, the

difference between direct and indirect band edges is so small that electrons can easily be transferred between these minimum with a small amount of thermal energy.

Photoluminescence properties of GaSe have been widely studied [14, 42-52], but there are still discrepancies between experimental findings and their explanation. This is in part due to the difficulties encountered in growing perfect single crystals with well known stacking type, and in part due to the difficulties in understanding the light emission from both direct and indirect nature of the bandgap of GaSe. In general, the PL spectra of GaSe consist of a series of lines which spread over a region of about 50 meV lying immediately below the free exciton (FE) line. These lines were attributed to different mechanisms including bound exciton from both direct and indirect band edges [44, 45], and the presence of different polytypes in the same sample [41].

One of the PL spectra of the GaSe samples grown at our laboratory is seen in Fig. (4.7). This spectrum was obtained with an incidence of 45° with respect to the crystal axis (case 1 below) angle. The PL peaks are strongly depending on the angle of incidence of the laser beam due to the anisotropy in the crystal. We discuss the anisotropy in the next sections. We see that several PL peaks have overlapped. We have deconvoluted these peaks by using a commercially available computer program. Deconvoluted peaks are shown in Fig. (4.7). At ~ 20 K we identify 2 peaks with energies 2.086 eV, 2.067 eV, respectively. The peak with the highest energy is obviously corresponding to the FE of the direct band edge. The activation energy analysis of this exciton peak is given in the next section. From this analysis we find the binding energy to be 27.1 meV which is consistent with the reported values [45]. This activation energy is almost same are the energy difference between two peaks

(~20 eV). The bandgap of the crystal is then found to be 2.113eV. This value is almost same as the known bandgap of GaSe.

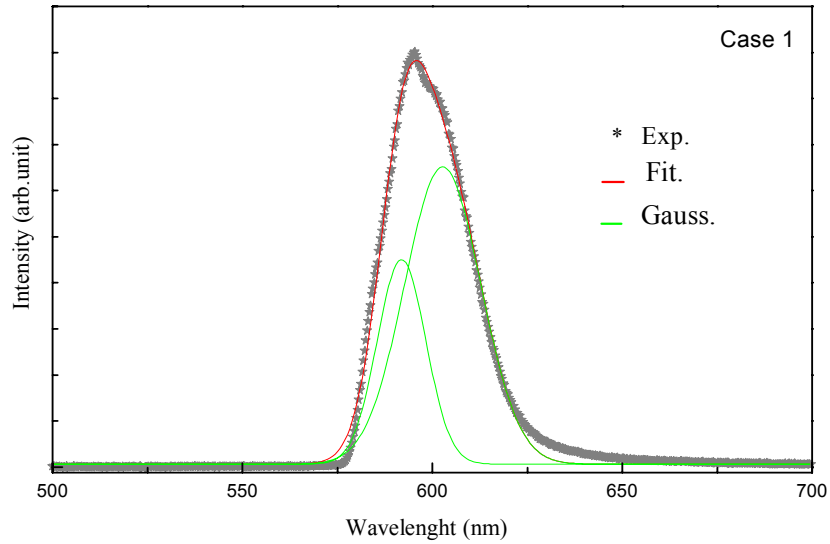


Fig.4.7 Deconvolution of the photoluminescence spectra into Gaussian lineshapes at ~20 K. (k//c)

Table.3.2.1 Peak energy values of GaSe comparing with the literature.

For our work at 70K	Case 1	2.084 eV	2.050 eV	-
	Case 2	2.047 eV	1.976 eV	1.919 eV
[42]	at 77 K	2.103 eV	2.075 eV	2.037 eV
[43,44 ,45]	at 77 K	2.098 eV	2.078 eV	2.035 eV
[46,47 ,48] 1999,1993 at 77 K	1991	2.098 eV	2.036 eV	-
		2.100 eV	2.030 eV	-
[49]	at 77 K	2.109 eV	-	-
[50]	at 78 K	2.100 eV	-	-
[51]	at 77 K	2.098 eV	2.098 eV	2.029 eV

The energy values of the observed PL peak and their relative distance to FE peak are shown in Table. (3.2.1). Due to the optical anisotropy the emission is

strongly depending on the angle of laser incidence and the detector position. Case 1 and Case 2 correspond two experimental conditions as will be described later. The peak energy position obtained from these two cases is displayed in the table. Similar, peak values reported in the literature are also shown for comparison. We see that the energy values determined from the peak position of the PL spectrum are in agreement with the values measured by others. From the thermal quenching experiments presented in the next section, we can conclude that these two PL peaks (case 1) resulted from the free exciton and bound exciton connected direct band edge. If they were originating from different polytypes, we would expect no variation in the relative intensities of the PL peaks.

4.3.1 Temperature dependence of PL spectra

Temperature dependence of PL spectra provides information on the source of illuminating centers. As described in the previous section, the variation of the bandgap with temperature is obtained from the temperature variation of the band-to-band transition. Also the energy position of the illuminating center can be determined from the activation energy analysis of the PL peaks.

Fig. (4.8) shows the plot of FE peak energy intensity versus $1/kT$. The slope of the line fitted to the straight line part of this graph gives the activation energy of the FE dissociation. It thus gives the energy difference between FE energy level and the conduction band edge. We have determined this energy to be 26.4 meV from this slope as indicated in Fig. (4.8). The bandgap energy is then found by adding this activation energy to the peak energy of the PL peak. The room temperature bandgap value is found to be 2.021 eV.

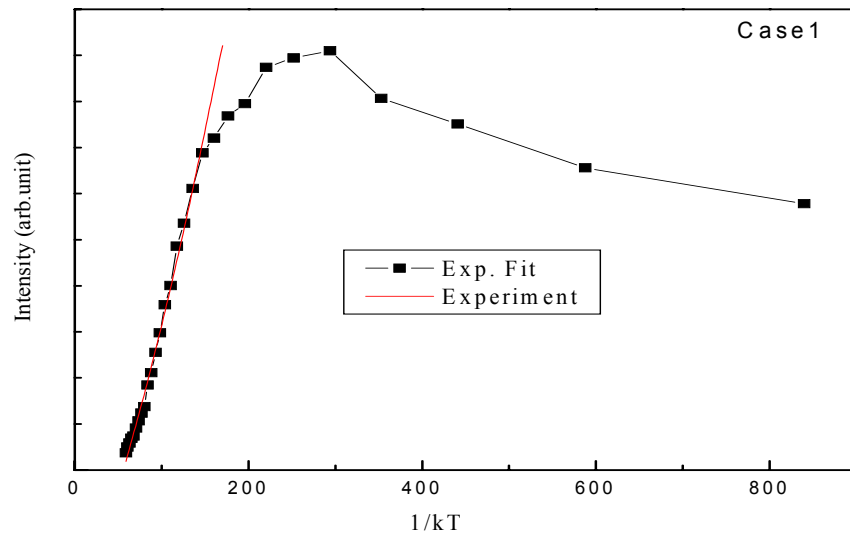


Fig.4.8 Variation of GaSe PL intensity with reciprocal temperature, at 20 and 300 K.

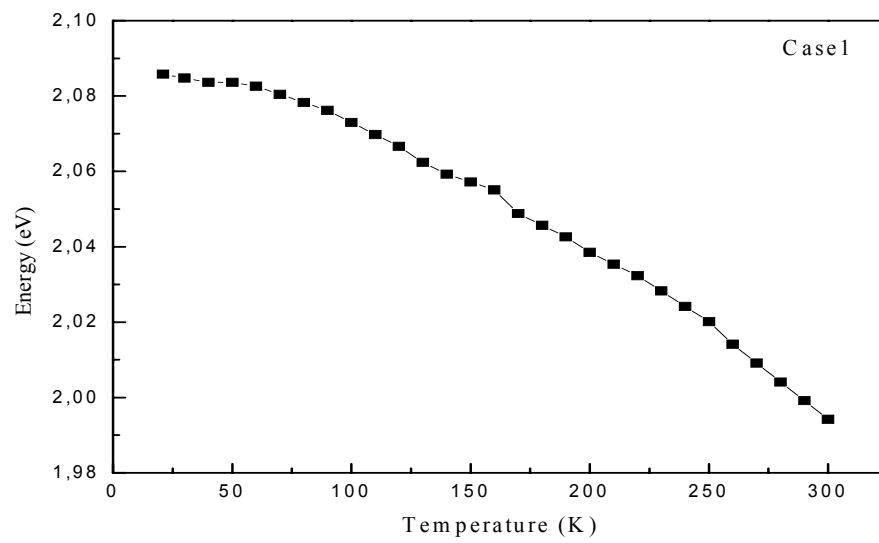


Fig.4.9 Temperature dependence of the peak energy position of the A band.

Fig.(4.9) shows the temperature variation of the A band energy in the temperature range of 20 - 300 K. As expected the bandgap increases with decreasing temperature with commonly observed characteristics. The A band shifts towards the red. It is a general practice to explain the bandgap variation by

$$E_g(T) = E_g(0) - \frac{\alpha T^2}{T + \beta}$$

where $E_g(0)$, α and β are fitting parameters. These parameters are extracted from the Fig. (4.9) by making linear fit and the obtained values are 2.11 eV, 3.34×10^{-4} and 0.14, respectively.

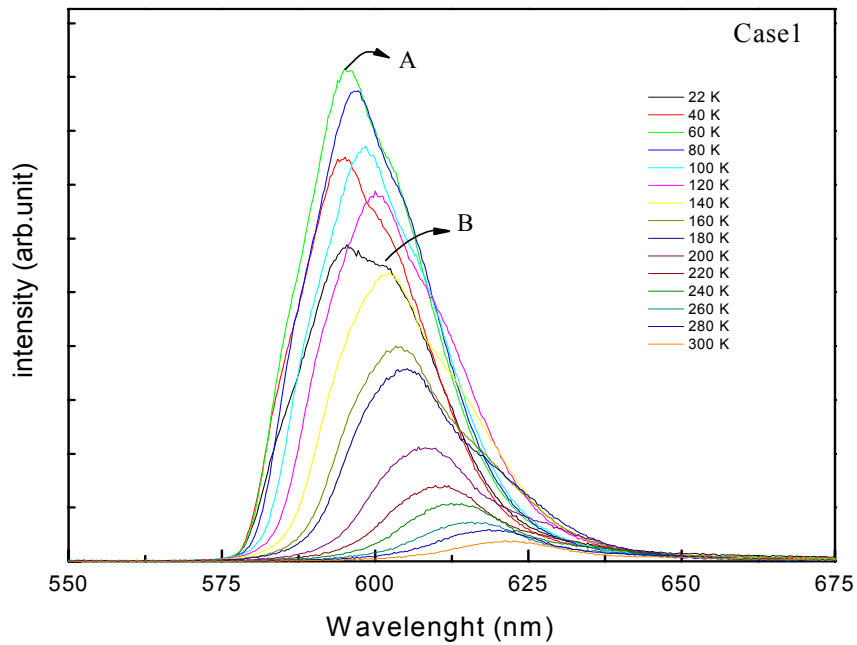


Fig.4.10 Photoluminescence spectra of undoped p-type GaSe as a function of temperature. k/c.

From Fig. (4.10), it can be seen that the intensities of A and B bands decrease with increasing temperature with the A band quenching much more rapidly than the B band. The variations in the PL peak intensities of A band and B band with

respect to reciprocal temperature are plotted in Fig. (4.8). In the low-temperature range, the PL intensities of both bands decrease slowly. Above 160 K for A band and 70 K for B band, the rate of intensity decreases for both bands increase significantly owing to the thermal quenching processes. The activation energies for both bands were obtained by fitting the high-temperature regions of data the following equation

$$I = I_0 \exp\left(\frac{\Delta E}{k_B T}\right),$$

where I is the PL intensity, I_0 is a proportionality constant and k_B is Boltzmann's constant. The semilogarithmic plots of the peak intensity as a function of reciprocal temperature give straight lines in the 70-90 K regions for B band. The slope of these lines gives the activation energies as 27.1 eV for the B band. We conclude that this value is the dissociation energy of the bound exciton connected to the direct band edge.

4.3.2 Optical anisotropy in GaSe

As explained above, GaSe is a highly anisotropic material. The structural anisotropy results in anisotropy in the electrical and optical properties of GaSe. It has been reported that both light absorption and light emission properties show anisotropic behavior. This behaviour was found to result from the dependence of the transitions on the direction of the electric field vector with respect to the crystal axis. This dependence is a result of selection rules related to the anisotropic band structure of GaSe as discussed below. Anisotropy of GaSe was investigated by reflectivity measurements, where it was found that optical absorption is different for $E \perp c$ and $E // c$ [51]. We have studied the anisotropy in GaSe by measuring the PL emission in three different experimental configurations as shown in Figure 4.11.

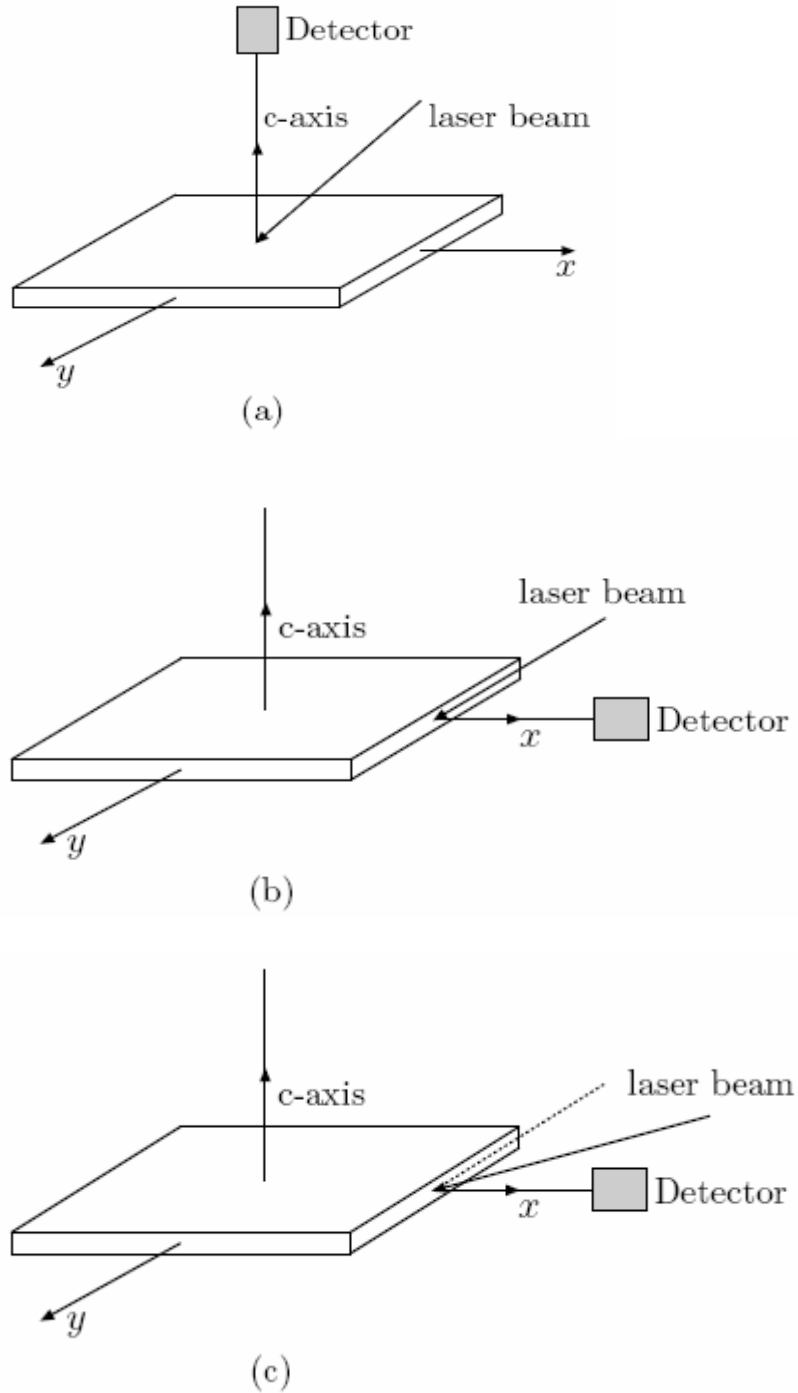


Fig.4.11 Experimental conditions for the measurement of anisotropic PL emission. a) Laser beam is directed to the sample surface with an angle of 45° with respect to c -axis. The detector is positioned along the c -axis ($k//c$). b) Laser beam is directed on the side of the sample. The detector's position is along the direction perpendicular to the c -axis ($c \perp k$). c) The detector is in the same position as b), but the laser beam falls on the sample with an angle.

In the first case (case 1), Fig. (4.11.a), laser is directed to the sample with an angle of incidence of 45° relative to the c-axis, and the detector is placed at a position where it measures the light propagating parallel to the c-axis ($k//c$). The majority of the detected light has therefore an electric field vector which is perpendicular to the c-axis, In the configuration (case 2) Fig. (4.11.b), the light beam is directed on to the crystal from its side so that the wave vector (k) of the light is perpendicular to the c-axis. The detector faces the crystal side and measures the light having a wave vector perpendicular to the c-axis ($k \perp c$). In the third case (case 3), the detector's position is along the direction perpendicular to the c-axis, but the light beam is impinged on the sample with an arbitrary angle as shown in Fig. (4.11.c). This work represents the first study that uses the experimental conditions described here.

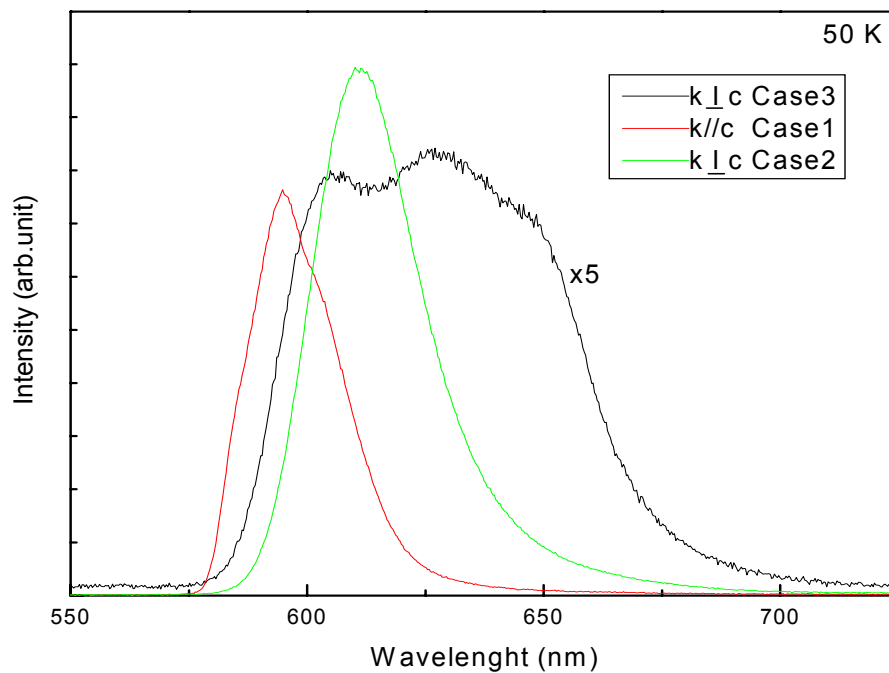


Fig.4.12 Photoluminescence spectrum of GaSe with respect to $k//c$ and $k \perp c$ axis.

Fig. (4.12) Shows the PL spectra for the three measurement conditions described above at temperatures given on the figure. We see surprising differences between the three measured spectra. For $c//k$, where electric field vector is perpendicular to the c axis ($E \perp c$), a PL band with some overlapped peaks is seen at an energy which is higher than the energy of the PL band measured with other two configurations. This result demonstrates the strong optical anisotropy in GaSe. In order to understand the physical mechanisms behind these emissions, their temperature variations were studied and are shown in Fig. (4.10), (4.13) and (4.14). The results reflect the complicated nature of the optical absorption and emission processes in GaSe crystal. In the previous studies on PL characteristics of GaSe, differences between $E \perp c$ and $E//c$ were observed and explained by considering the band structure [42, 51]. The present results are partly in agreement with these previous results. Owing to new information provided by the new experimental conditions, some of the unique features observed in this work are reported for the first time. These features need to be explained and compared with the other published results.

Optical anisotropy in GaSe was explained by considering its electronic band structure [51]. According to the band structure calculation, energy position of p_x , p_y , and p_z states are not the same. p_z valence band states is situated slightly higher energy than $p_{x,y}$ states. It was suggested that the transition with ($E//c$) is derived from the bonding-antibonding bands of the p_z orbitals, while the transitions with $E \perp c$ is derived from the $p_{x,y}$ antibonding (valence) band and the p_z antibonding (conduction) band. Selection rules require that transitions for $E \perp c$ are allowed only between bands having the same parity and the transition for $E//c$ are allowed only between

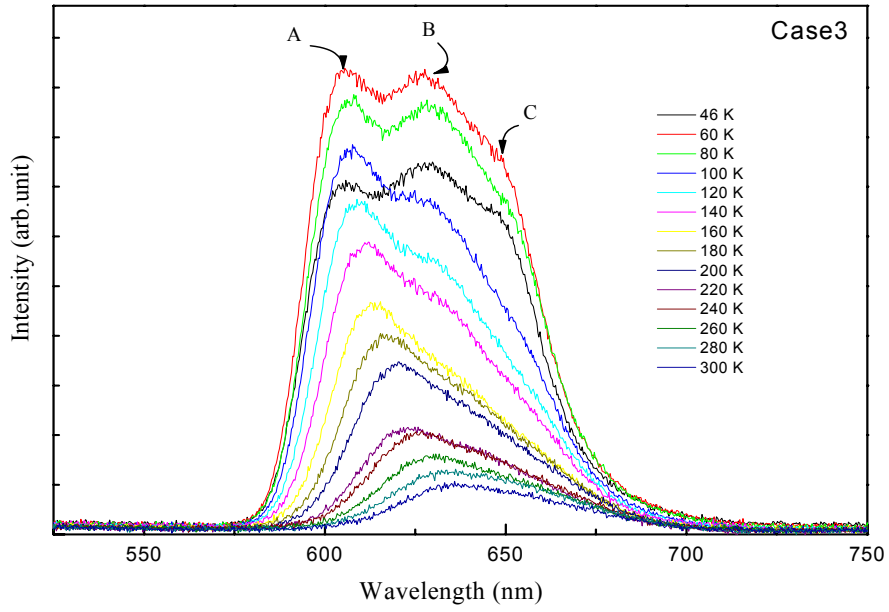


Fig.4.13 Photoluminescence spectra of GaSe as a function of temperature ($k \perp c$).

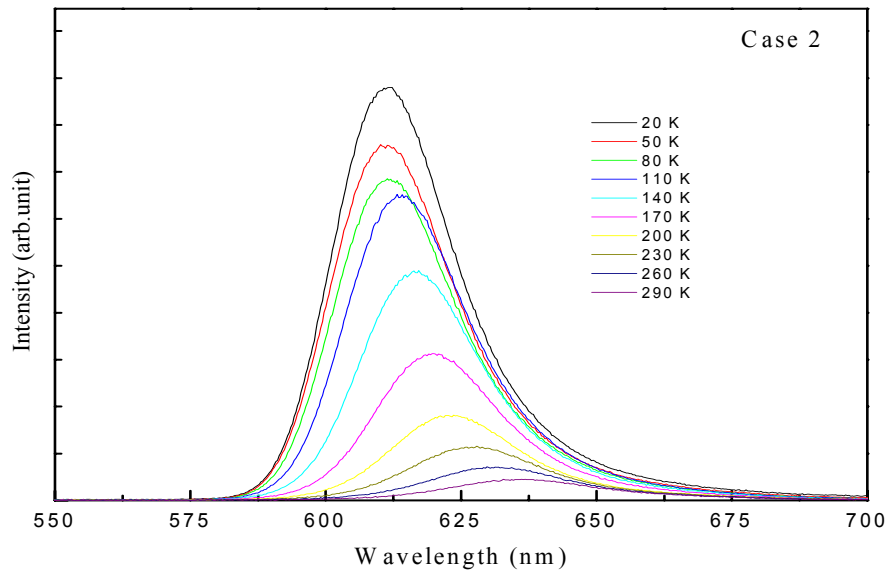


Fig.4.14 Photoluminescence spectra of GaSe as a function of temperature ($k \perp c$).

bands having opposite parity. One can then understand that the high energy peak observed in the first case (Fig.4.12), where $k//c$ and $E \perp c$, is due to the allowed transitions between antibonding states of $p_{x,y}$ and p_z bands. In the second measurement condition, $k \perp c$ and the perpendicular component of electric field is weak. The transitions with low energy emission dominate the PL spectra in this case due to smaller energy difference between p_z states. An interesting feature of this second case is that the PL band consists of a single peak which does not appear to be a combination of several other peaks. Although the asymmetry in the PL band indicates the existence of different peaks within the main PL band, these peaks are not resolvable. It is likely that one of the transitions dominates the whole PL emission and gives the observed spectra. This conclusion is supported by the results obtained in case 3 in which the laser beam is directed with an angle while the detector position is kept same. As shown in Fig. (4.12), the emission intensity drops significantly and different emission peaks are resolvable. This suggests that high emission intensity in the second case is related to the dominance of the absorption/emission of the light with $k \perp c$.

It is interesting to study the energy position and the temperature dependence of the peaks resolved in case 3 (Fig.4.17). In table 3.2, we have displayed the energy values of the peaks deconvoluted from the band shown in Fig.(4.15) along with the energy of the peaks observed in case 1 ($E \perp c$). The energy difference between the peaks is also shown to see the possible energy separation between the illuminating centers. As discussed above, the observed two peaks are believed to result from the free and bound exciton transitions in the first case. The energy difference is 0.034 eV (at 70 K) between the peaks and these values are in close agreement with those

published by others. However we see an interesting situation in the third condition. The energy differences between the peaks are 0.070 eV and 0.056 eV which are larger than those obtained in the first case.

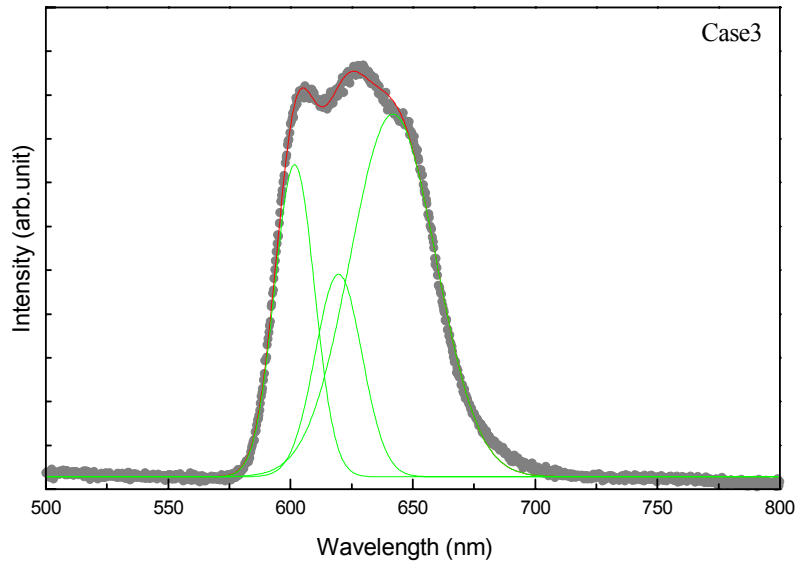


Fig.4.15 Deconvolution of the photoluminescence spectra into Gaussian lineshapes at ~ 20 K. ($k \perp c$)

A plot of peak intensity vs. $1/kT$ for the two resolved peaks is shown in Fig. (4.16). In the low temperature range, the PL intensities of both bands decrease slowly. The activation energies for two bands have been obtained by fitting the high-temperature regions of the data. The semilog plots of the peak intensity as a function of the reciprocal temperature give straight lines in the 120-300 K. The slopes of these lines give the activation energies as 26.4 meV and 24.5 meV for A and B bands, respectively.

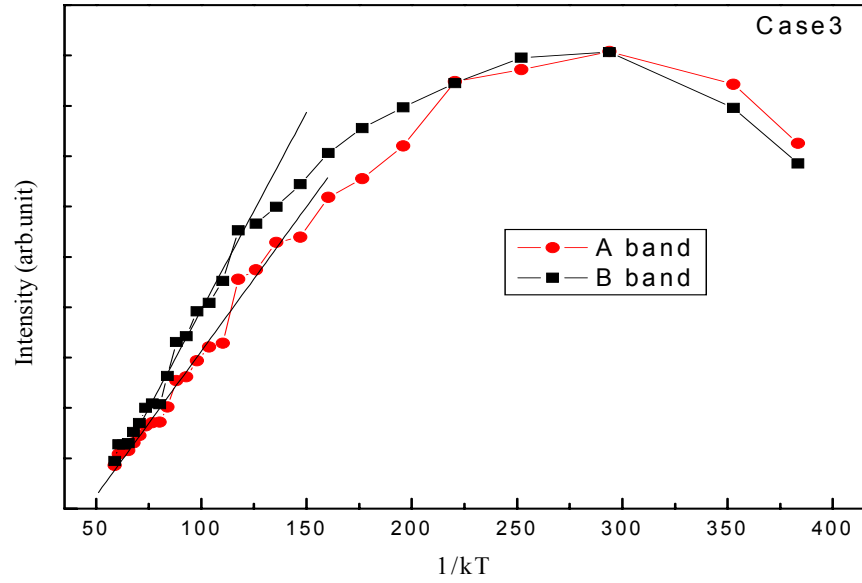


Fig.4.16 Variation of GaSe PL intensity with reciprocal temperature ($k \perp c$).

Temperature dependence of peak energy for all peaks is plotted in Fig. (4.17). A and B band peak energies decreases as the temperature increases. Changes in the peak energy position shifts lower energies as the temperature increases.

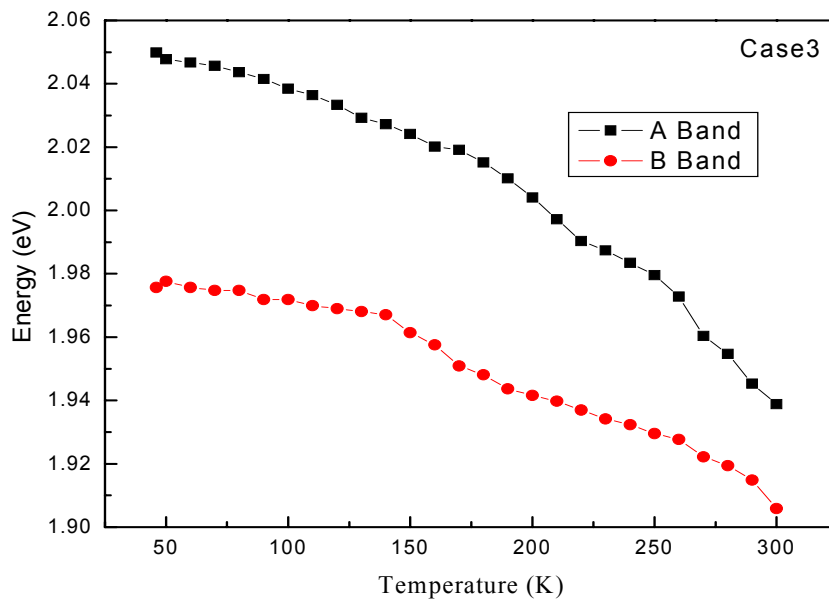


Fig. 4.17 Temperature dependence of the peak energy position ($k \perp c$).

CHAPTER 5

CONCLUSION

Optical properties of semiconductors have been important both from technological and scientific point of view. Semiconductors emit light in a controllable manner. One can fabricate devices emitting ordinary light or LASERs in the visible and infrared region of the spectrum. These devices are used in variety of applications such as telecommunication, home electronics, industrial and space applications. In addition to these technological applications, the study of light emission provides scientific information about the material being studied. As widely discussed throughout this thesis, basic electronic structure of the material as well as the defect centers can be revealed by studying the luminescence properties.

Two interesting semiconductors CdS and GaSe have been studied in this work. Another aim of this work was to study the photoluminescence spectroscopy as an experimental technique. The experimental set-up for PL spectroscopy has been improved in the course of this M.Sc study. New experimental approaches have been adapted to measure the optical anisotropy. The study on CdS and GaSe has been very exciting due to the interesting features of these materials and also due to the new insights they brought into the PL spectroscopy.

CdS, being II-VI semiconducting compound, has some interesting properties which make it a beneficial material in optoelectronic devices. The florescent spectra of CdS exhibit extremely complex behaviour. We investigated the photoluminescence of CdS as a function of temperature. We observed three bands, namely the green, the red, and Raman. In our analysis green band of CdS has five peaks centered in the region 490 – 537 nm with peak energy values 2.53 eV, 2.41 eV, 2.37 eV, 2.33 eV, and 2.30 eV, respectively. In the red band, the peak energy appears at 696 nm of the value 1.78 eV which overlaps with the prediction of studies in literature. Raman peak was found at 449 nm with peak energy 2.76 eV in the temperature range 20 – 130 K. We suggested that, in the green band, PL1 is interpreted as free exciton, PL2 as bound exciton, PL3 as transition from conduction band to acceptor state, PL4 as transition from donor level to the valance band, and the last one (PL5) as the donor-acceptor transition. These peaks except PL1 survive 20 – 70 K. The red band is likely to be the transition through the deep level created by S vacancies.

For GaSe, photoluminescence spectra were studied as a function of temperature by considering three cases which are classified according to the angle of incidence of the laser light and detector position. The layer compound GaSe is characterized by a strong structural anisotropy with respect to one crystal axis: it consists of thin tightly bound layers which are stacked on top of each other and the cohesion between the layers is relatively weak when we compare the cohesion in a layer. Thus, as expected, different experimental conditions defined above given us strongly anisotropic energy spectra for the emission. We investigated PL spectra of

GaSe within the temperature range 20 - 300 K by means of N₂ laser with constant intensity.

For the case $E \perp c$, two broad peaks were observed with energies 2.086 eV, 2.067 eV at around 594 and 600 nm, respectively, in the lowest accessible temperature (~ 20 K). Both peak energy positions decrease as temperature increases. Unlike the first peak (A band), the second one (B band) was seen in temperature range 20 – 90 K but we are still able to barely identify the existence of B band up to room temperature. We decided that A band is most likely to result in free excitons and similarly B band is probably originated by bound exciton.

After having discussed the case $E \perp c$, we dealt with the $E // c$ case by further considering two subcases, the k vector parallel to the edge of the crystal (second case) and making an angle (third case). In the first subcase there exists one peak in the spectrum with energy 2.027 eV, 612 nm, at 20 K. In the second subcase we observed three peaks having energies 2.046 eV, 1.975 eV, and 1.911 eV with centered 606 nm, 627nm, and 649 nm at 70 K, respectively. The behaviour of peak energy positions shows the characteristic with those in the first case ($E \perp c$).

The energy difference between peaks, related to the energy differences among illuminating centers, is 0.034 eV for the case ($E \perp c$), and 0.070 eV and 0.056 eV for the third case ($E // c$), which are larger than that of the first case.

The observed optical anisotropy can be understood by considering the band structure of the GaSe crystal. It was suggested that energy differences in the valence and conduction band states and the selection rules that govern the absorption results in the anisotropy observed in the PL emissions.

REFERENCES

- [1] Linhtowlers in *Growth and characterization of semiconductors*, ed.by R. A. Stradling and P.C.Klippstein, Bristol 1990, p. 135.
- [2] C.B. Collins, R. O. Carlson and C.J. Gallagher, *Phys.Rev.***105**, 1168, (1957).
- [3] L.Ward, “Cadmium Sulfide”, in *Handbook of Optical Constant of Solids*, Vol.2, edited by E.D. Palik p.579, (Academic press, Boston, 1991).
- [4] S.S. Devlin, “*Transport Properties*”, in *Physics and Chemistry of II-VI compounds*, edited by M. Aven and J.S. Prener, (North-Holland, Amsterdam, 1967).
- [5] J.L. Pankove, *Optical Processes of Semiconductors* (Dover, New York, 1971).
- [6] A.G. Kyazym-zade, R. N. Mekhtieva, and A.A. Akhmedov, *Sov. Phys. Semiconductors* **25**, 840, (1992)
- [7] M. Schluter, *Nuovo Cimento* **13B**, 313, (1973)
- [8] F. Hulliger, *Structural Chemistry of layer type phases* (1976)
- [9] A. Mercier and J. P. Voitchovsky, *J. Phys. Chem. Solids* **36**, 1411, (1975).
- [10] J. Singh, *Semiconductors optoelectronic*, McGraw-Hill Press, pp.75 (1995).
- [11] S. Sze, *Physics of semiconductor devices*, 2nd ed., JW&S, pp.848-849.
- [12] T. Tambo and C. Tatsuyama, *Surface Science* **222**, 343 (1989).
- [13] K. Uneo, K. Saiki, A. Koma, *Jap. J. Appl. Lett.***30**, L1352 (1991).
- [14] V. Capozzi, *Phys Rev B* **28**, 4260 (1983).
- [15] A. Kuhn, A. Chevy, and R. Chevalier, *Phys. Stat. Sol.(a)* **31**, 469 (1975).

- [16] Y. Depeursinge, *Nuova Cimento* **64B**, 111 (1981).
- [17] M. K. Anis, PhD thesis Brighton Polytechnic England (1977).
- [18] C. R. Whitehouse, PhD thesis Brighton Polytechnic England (1977).
- [19] M. Schluter, *Nuova Cimento* **13B**, 313 (1973).
- [20] Y. Depeursinge, thesis no 297, Ecole polytec. Federela Lausanne, Switzerland (1978).
- [21] N. C. Fernelius, *Prog. Crystal Growth and Charact. Of Materials* **28**, 275-353 (1994).
- [22] A. M. Ferendeci, *solid state and electron devices*, pp.118 (1991)
- [23] S. O. Kasap, *Principle of Electrical Engineering Material and Devices*, pp320 (1997).
- [24] Y. Yu, M. Cardona, *Fundamentals of Semiconductors*, pp.348, springer, Berlin (1995).
- [25] H. K. Schröder, *Semiconductor Material and Device Characterization*, New York, John Willey & Sons, Inc., 624, (1998).
- [26] H B. Bebb and E. W. Williams, *Semiconductors and Semimetals*, Vol.8, (1972).
- [27] P. J. Dean, *Prog. Cryst. Growth Charact.* **5**, 89 (1982).
- [28] T. Taguchi, J. Shirafuji, and Y. Inuishi, *Pyhs. Status Solidi B* **68**, 727 (1975).
- [29] Q.Kim and D.W. Langer, *Pyhs. Status Solidi B* **122**, 263 (1984).
- [30] T. Schmit, H Sitter and K. Lischka, *J. Cryst. Growth* **101**, 190 (1990).
- [31] M. Agata *Solid State Communication* **76**, 1061 (1990).
- [32] D. C. Thomas, and J.J. Hopfield, *Phys. Rev.***128**, 2135, (1962).
- [33] N. V. Starostin, *Opt. Spectros.* **75**, 770, (1998).
- [34] C. H. Henry, R. A. Faulkner and K. Nassau, *Phys. Rev.* **183**, 798, (1969).

- [35] N. Susa, Jpn. Appl. Phys. **15**, 2365 (1976).
- [36] B. A. Kulp, Phys. Rev. **125**, 1865 (1962).
- [37] J. Humemberger, Thin Solid Films **121**, 75 (1984).
- [38] N. S. Bogdanyuk, Semiconductors **29**, 181 (1995).
- [39] O. Vigil, J. Vac. Sci. Technol. A, **15**, 2282, 1997.
- [40] C. Mejia-Garcia et. al., J. Appl. Phys. **86**, 3171 (1999).
- [41] Y. Fan, T. Schittkowski, M. Bauer, L. Kador, K. R. Allakhverdiev, E. Yu. Salaev, J. of Luminescence **98**, 7, (2002).
- [42] J. P. Viotchovsky, A. Mercier , Nuovo Cimento **22** , 273 (1974).
- [43] V. Capozzi, M. Montagna , Phys. Rev.B **40**, 3182 (1989).
- [44] V. Capozzi, Phys. Rev. B **23**, 836 (1981).
- [45] V. Capozzi, S. Caneppele, M. Montagna, F. Levy, Phys. Stat. Sol. B **129**, 247 (1985).
- [46] S. Shigetomi, T. Ikari , Philosophical Magazine Letters **799**, 575 (1999).
- [47] S. Shigetomi, T. Ikari, H. Nakashima, J. Appl. Phys. **74**, 4125 (1993).
- [48] S. Shigetomi, T. Ikari, H. Nakashima, J. Appl. Phys. **74**, 4125 (1993).
- [49] S. Shigetomi, T. Ikari, H. Nishimura, J. Appl. Phys. **69**, 7936 (1991).
- [50] J.L. Brebner, E. Mooser, Phys. Letters **24A**, 274 (1967).
- [51] W. Y. Liang, J. Phys. C: Solid State Phys. **8**, 1763 (1975).
- [52] B. G. Tagiev, G. M. Niftiev, and S.A. Abushov, Phys. Stat. Sol.**B121**, K195 (1984).

APPENDIX A

In this appendix we will give some details of momentum matrix element calculation for an electron moving in an electromagnetic field discussed in chapter 2.

In the dipole approximation mentioned in chapter 2 the momentum matrix element for an initial state i to final state n is given by

$$\vec{p}_{in} = \frac{\hbar}{i} \int d^3r \psi_{nl}^*(\vec{r}) \vec{\nabla} \psi_{il}(\vec{r}), \quad (\text{A1})$$

where l' and l represent the band indices. If we use the Bloch function form of the states, we can choose as

$$\begin{aligned} \psi_{nl} &= e^{i\vec{k}_n \cdot \vec{r}} u_{nl}, \\ \psi_{il} &= e^{i\vec{k}_i \cdot \vec{r}} u_{il}, \end{aligned} \quad (\text{A2})$$

where u_{il} is the cell periodic part of the Bloch state and it has the same periodicity with background potential seen by the electrons. Then, \vec{p}_{in} becomes

$$\begin{aligned} \vec{p}_{in} &= -i\hbar \int d^3r e^{-i\vec{k}_n \cdot \vec{r}} u_{nl}^*(\vec{r}) \vec{\nabla} e^{i\vec{k}_i \cdot \vec{r}} u_{il} \\ &= -i\hbar \int d^3r e^{-i\vec{k}_n \cdot \vec{r}} u_{nl}^*(\vec{r}) \left[i\vec{k}_i e^{i\vec{k}_i \cdot \vec{r}} u_{il} + e^{i\vec{k}_i \cdot \vec{r}} \vec{\nabla} u_{il} \right] \\ &= \hbar\vec{k}_i \int d^3r \psi_{nl}^* \psi_{il} - i\hbar \int d^3r e^{i(\vec{k}_i - \vec{k}_n) \cdot \vec{r}} u_{nl}^* \vec{\nabla} u_{il}. \end{aligned} \quad (\text{A3})$$

We can use (A3) to determine the selection rules for band to band transition. The first term in (A3) is zero from the fact that Bloch states are orthogonal for different k

values. If we look the integrant in the second term, $u_{nl}^* \nabla u_{nl}$ is periodic with, say, period R. Then,

$$\begin{aligned} II &= -i\hbar \int d^3 r e^{i(\vec{k}_i - \vec{k}_n)(\vec{r} + \vec{R})} u_{nl}^* \vec{\nabla} u_{il} \\ &= e^{i(\vec{k}_i - \vec{k}_n)\vec{R}} II \end{aligned} \quad (\text{A4})$$

(A4) says that $(\vec{k}_i - \vec{k}_n) \cdot \vec{R} = 0$ which gives us $\vec{k}_i = \vec{k}_n$. This means that interband transitions are vertical. Therefore, the momentum matrix element becomes

$$\overline{P}_{in} = -i\hbar \int d^3 r u_{kl}^* \vec{\nabla} u_{kl}. \quad (\text{A5})$$

To calculate momentum matrix element let us consider the near bandedge transitions from a state in the conduction band to a state in the valance band. Central cell part of the electronic state can be a pure combination of only s-type states (l=0) or only p-type states (l=1) for certain special k values. The central cell part of the electrons at the bottom of the conduction band of direct bandgap materials (k=0) is purely s-type and let's denote it as $|s\rangle$, i.e., $u_{c0} = |s\rangle$. As final states, there are four possible states, two of which are denoted as heavy hole states (HH) and the others as light hole states (LH). Let us express the states formed by including both orbital and spin angular momentum of the electron. If we denote total angular momentum as $\vec{J} = \vec{L} + \vec{S}$, they limits for total principle quantum member j is

$$|l - s| \leq j \leq |l + s|, \quad (\text{A6})$$

where l and s are the orbital and spin quantum numbers respectively. The possible values for j of a p-state (l=1) electron ($s = \frac{1}{2}$) are

$$j = \frac{3}{2}, \frac{1}{2}, \quad (\text{A7})$$

and for each j there are $2j+1$ m_j values. The possible states $|j, m_j\rangle$ are $|\frac{3}{2}, \frac{3}{2}\rangle$, $|\frac{3}{2}, \frac{1}{2}\rangle$, $|\frac{3}{2}, -\frac{1}{2}\rangle$ and $|\frac{3}{2}, -\frac{3}{2}\rangle$ for $j = \frac{3}{2}$, and $|\frac{1}{2}, \frac{1}{2}\rangle$ and $|\frac{1}{2}, -\frac{1}{2}\rangle$ for $j = \frac{1}{2}$. The states $|\frac{3}{2}, \pm\frac{3}{2}\rangle$ are called as HH states, $|\frac{3}{2}, \pm\frac{1}{2}\rangle$ as LH states, and $|\frac{1}{2}, \pm\frac{1}{2}\rangle$ as split-off states. We will deal with near bandedge transitions. Thus only HH and LH states are considered in the valance band. From the theory of addition of angular momenta we can expand the $|j, m_j\rangle$ states as an expansion of $|l, m_l\rangle|s, m_s\rangle$ direct product states of the form

$$|j, m_j\rangle = \sum_{m_l, m_s} C(m_l, m_s) |l, m_l\rangle |s, m_s\rangle, \quad (\text{A8})$$

where $C(m_l, m_s)$ is called as Clebsh-Gordon coefficients and they are nonzero if $m_j = m_l + m_s$ is satisfied. For $j = \frac{3}{2}, m_j = \frac{3}{2}$ state there is only one combination as

$$\begin{aligned} |\frac{3}{2}, \frac{3}{2}\rangle &= C(1, \frac{1}{2}) |1, 1\rangle |\frac{1}{2}, \frac{1}{2}\rangle \\ &= |1, 1\rangle |+\rangle, \end{aligned} \quad (\text{A9})$$

where the Clebsh-Gordon coefficient is 1 from normalization and $|+\rangle$ denotes spin-up state. Similarly for $j = \frac{3}{2}, m_j = -\frac{3}{2}$ case

$$|\frac{3}{2}, -\frac{3}{2}\rangle = |1, -1\rangle |-\rangle, \quad (\text{A10})$$

where $|-\rangle$ represents $|\frac{1}{2}, -\frac{1}{2}\rangle$ spin-down state. The LH states are

$$\begin{aligned} |\frac{3}{2}, \frac{1}{2}\rangle &= C(1, -\frac{1}{2}) |1, 1\rangle |-\rangle + C(0, \frac{1}{2}) |1, 0\rangle |+\rangle, \\ |\frac{3}{2}, -\frac{1}{2}\rangle &= C(-1, \frac{1}{2}) |1, -1\rangle |+\rangle + C(0, -\frac{1}{2}) |1, 0\rangle |-\rangle, \end{aligned} \quad (\text{A11})$$

where we have to determine the Clebsh-Gordon coefficient by using normalization and orthogonality of states. The normalized states become

$$|\frac{3}{2}, \frac{1}{2}\rangle = \frac{1}{\sqrt{3}} [|1, 1\rangle |-\rangle - 2 |1, 0\rangle |+\rangle],$$

$$|\frac{3}{2}, -\frac{1}{2}\rangle = \frac{1}{\sqrt{3}} [|1, -1\rangle |+\rangle + 2|1, 0\rangle |-\rangle]. \quad (\text{A12})$$

Furthermore, the angular part of the states, $|l, m_l\rangle$, can also be expressed in terms of three independent p-functions which are p_x, p_y and p_z . Since a spherical tensor can be expressed in terms of components of some vectors, by calling $\sqrt{\frac{3}{4\pi}} \frac{r_i}{r}$ as p_i ,

$i = x, y, z$ we get

$$\begin{aligned} |1, 1\rangle &= -\frac{1}{\sqrt{2}} [p_x \rangle + i | p_y \rangle], \\ |1, -1\rangle &= \frac{1}{\sqrt{2}} [p_x \rangle - i | p_y \rangle], \\ |1, 0\rangle &= | p_z \rangle. \end{aligned} \quad (\text{A13})$$

The non zero elements from the conduction band to the valance band are only

$$\langle p_x | p_x | s \rangle = \langle p_y | p_y | s \rangle = \langle p_z | p_z | s \rangle = p_{cv}, \quad (\text{A14})$$

where the equality is clear from symmetry. Consequently, the allowed transitions for

HH states $|HH\rangle = |\frac{3}{2}, \frac{3}{2}\rangle$ are

$$\begin{aligned} \langle HH | p_x | s \rangle &= -\frac{1}{\sqrt{2}} [\langle p_x | + i \langle p_y |] p_x | s \rangle \\ &= -\frac{1}{\sqrt{2}} \langle p_x | p_x | s \rangle = -\frac{p_{cv}}{\sqrt{2}}, \end{aligned}$$

$$\begin{aligned} \langle HH | p_y | s \rangle &= \frac{1}{\sqrt{2}} \langle p_y | p_y | s \rangle \\ &= \frac{1}{\sqrt{2}} \langle p_x | p_x | s \rangle = \frac{p_{cv}}{\sqrt{2}}, \end{aligned}$$

$$\langle HH | p_z | s \rangle = 0, \quad (\text{A15})$$

and for $|HH\rangle = |\frac{3}{2}, -\frac{3}{2}\rangle$ case

$$\langle HH | p_x | s \rangle = \frac{1}{\sqrt{2}} p_{cv},$$

$$\begin{aligned}\langle HH|p_y|s\rangle &= \frac{i}{\sqrt{2}} p_{cv}, \\ \langle HH|p_z|s\rangle &= 0.\end{aligned}\tag{A16}$$

Similarly we can simply compute the matrix elements of momentum for HH states.

For $|LH\rangle = |\frac{3}{2}, \frac{1}{2}\rangle$ case

$$\begin{aligned}\langle LH|p_x|s\rangle &= -\frac{1}{\sqrt{6}} p_{cv}, \\ \langle LH|p_y|s\rangle &= \frac{i}{\sqrt{6}} p_{cv}, \\ \langle LH|p_z|s\rangle &= \frac{2}{\sqrt{6}} p_{cv},\end{aligned}\tag{A17}$$

and for $|LH\rangle = |\frac{3}{2}, -\frac{1}{2}\rangle$

$$\begin{aligned}\langle LH|p_x|s\rangle &= \frac{1}{\sqrt{6}} p_{cv}, \\ \langle LH|p_y|s\rangle &= \frac{i}{\sqrt{6}} p_{cv}, \\ \langle LH|p_z|s\rangle &= \frac{2}{\sqrt{6}} p_{cv}.\end{aligned}\tag{A18}$$

Since we are dealing with matrix square of the operator $\hat{\varepsilon} \cdot \vec{p}$, it is better to examine

$|\langle n|\hat{\varepsilon} \cdot \vec{p}|i\rangle|^2$ for different polarizations.

For z-polarized light: $\hat{\varepsilon} = \hat{z}$.

$$\begin{aligned}|\langle HH|p_z|s\rangle|^2 &= 0 \\ |\langle LH|p_z|s\rangle|^2 &= \frac{2}{3} p_{cv}^2.\end{aligned}\tag{A19}$$

For x-polarized light: $\hat{\varepsilon} = \hat{x}$

$$\begin{aligned}|\langle HH|p_x|s\rangle|^2 &= \frac{1}{2} p_{cv}^2, \\ |\langle LH|p_x|s\rangle|^2 &= \frac{1}{6} p_{cv}^2.\end{aligned}\tag{A20}$$

For y-polarized light: $\hat{\varepsilon} = \hat{y}$

$$\left| \langle HH | p_y | s \rangle \right|^2 = \frac{1}{2} p_{cv}^2,$$

$$\left| \langle LH | p_y | s \rangle \right|^2 = \frac{1}{6} p_{cv}^2. \quad (\text{A21})$$